HHS Public Access

Author manuscript

Nature. Author manuscript; available in PMC 2017 January 28.

Published in final edited form as:

Nature. 2016 July 28; 535(7613): 505–510. doi:10.1038/nature18942.

Rapid signaling in distinct dopaminergic axons during locomotion and reward

MW Howe and **DA Dombeck**

Department of Neurobiology, Northwestern University, Evanston IL

Summary

Dopaminergic projections from the midbrain to striatum are critical for motor control, as their degeneration in Parkinson's disease results in profound movement deficits. Paradoxically, most recording methods report rapid phasic dopamine signaling (~100ms bursts) to unpredicted rewards, with little evidence for movement-related signaling. The leading model posits that phasic signaling in striatum targeting dopamine neurons drive reward-based learning, while slow variations in firing (tens of seconds to minutes) in these same neurons bias animals towards or away from movement. However, despite widespread acceptance of this model, current methods have provided little evidence to support or refute it. Here, using new optical recording methods, we report the discovery of rapid phasic signaling in striatum-targeting dopaminergic axons that was associated with, and capable of triggering, locomotion in mice. Axons expressing these signals were largely distinct from those signaling during unexpected rewards. These results suggest that dopaminergic neuromodulation can differentially impact motor control and reward learning with sub-second precision and suggest that both precise signal timing and neuronal subtype are important parameters to consider in the treatment of dopamine-related disorders.

Introduction

Dopaminergic projections from substantia nigra pars compacta (SNc) to striatum are critical for motor control, as their degeneration in Parkinson's disease (PD) results in profound movement deficits[1–3]. However, little evidence for movement-related dopamine signaling has been observed; instead, most recording methods report phasic signaling (hundreds of millisecond bursts) to unpredicted rewards, which are superimposed on slowly varying background activity[4–10]. The leading model to explain dopamine's dual role in reward and movement posits that phasic bursts in striatum targeting dopamine neurons act to drive reward-based learning, while slow variations in firing (tens of seconds to minutes) in these

Correspondence: Mark Howe markhowe72@gmail.com or Daniel Dombeck d-dombeck@northwestern.edu.

Contributions

M.H. performed the experiments, D.D. built the experimental apparatus, M.H. performed data analysis with strategy suggestions from D.D. Both authors conceived and designed the experiments, interpreted the data and wrote the paper.

Competing financial interests

The authors declare no competing financial interests.

same neurons bias the system towards or away from movement[11–15]. However, current methods have provided little evidence to support or refute this model.

Most information about *in-vivo* dopamine dynamics comes from extracellular single unit recordings in the ventral tegmental area (VTA) and SNc[6–8,16–21] (Supplemental Discussion). This approach provides functional characterization of individual neurons with single-spike temporal resolution, but it cannot discriminate neurons by their projection targets. Moreover, midbrain single unit recordings alone cannot reliably discriminate dopaminergic from non-dopaminergic neurons[8,22] and are blind to the local control exerted on dopamine terminals in the target regions[23,24]. Fast-scan cyclic voltammetry (FSCV), on the other hand, measures changes in dopamine release directly in striatal terminal regions, but these measurements of extra-synaptic dopamine, averaged over hundreds of microns, are insensitive to synaptically confined dopamine and potentially heterogeneous signaling across different axons[25]. To measure both phasic (hundreds of millisecond) and slowly varying (tens of seconds to minutes) dopamine signaling in the striatum during reward delivery and animal movement, and to determine whether dopamine projections to striatum broadcast homogenous or heterogeneous signals, we used two-photon calcium imaging and fiber photometry to establish the striatal dopamine signaling patterns occurring in locomoting mice receiving unpredicted rewards. We then tested the role that these activity patterns play in motor control by optogenetically stimulating striatum targeting dopamine axons.

Locomotion related dopamine signaling

A new approach was established to image the activity of dopamine projection axons in dorsal striatum (Fig 1a–d,[26]). DAT-cre mice (n=6) were injected in the midbrain with AAV1–Syn–flex–GCaMP6f[27], leading to specific expression of GCaMP6f in dopamine neurons widespread throughout SNc and VTA (Fig 1d). A chronic imaging window was then implanted over dorsal striatum (Extended Data Fig 1b) to enable two-photon imaging (Methods[26], Extended Data Fig 2i) of the GCaMP6f expressing dopaminergic projection axons (Fig 1c). Axons were clearly visible, but were densely packed (Fig 1c, Extended Data Fig 1a), presumably representing overlapping axonal arbors from numerous different dopamine neurons[28]. Mice were then head-restrained over a cylindrical treadmill and time-series movies of the labeled axons were acquired (in the dark) during rest, self-initiated locomotion, and/or delivery of unexpected rewards (Fig 1e).

Calcium influx into axons and terminals, caused by axonal action potentials[29,30] (with local modulation possible[23,24]), triggers neurotransmitter release[31–33], and therefore, changes in GCaMP6f fluorescence[27] provide an indirect measure of dopamine release in dorsal striatum[34]. These GCaMP6f fluorescence changes are well-suited for determining whether mouse locomotion (100s of millisecond timescale accelerations) is associated with rapid phasic dopamine signaling (sub-second-duration GCaMP6f transients), slowly varying dopamine signaling (tens of seconds to minutes-duration transients or changes in baseline) or both (Methods, Extended Data Fig 3a–c).

As a first metric to quantify dopamine signaling in dorsal striatum, we summed the fluorescence from all dopamine axons in each frame of each imaging field (60–250μm

diameter fields sampled at 28Hz) to generate a mean fluorescence activity trace (mean change in fluorescence, DF/F trace; Fig 1e, bottom). These traces revealed frequent transients during treadmill locomotion (Fig 1e), which varied in duration and amplitude but generally occurred on sub-second timescales (mean duration 678, 460ms std; mean amplitude 126, 67% DF/F std; Extended Data Fig 2g,h, 3e). Longer duration transients often contained multiple peaks, as expected from summation of closely spaced, short duration transients (Fig 1e, Extended Data Fig 3)[27]. Transients were typically synchronous across the densely innervated fields, presumably reflecting widespread co-activation of many projection axons (Extended Data Fig 1), and were more frequent during spontaneous locomotion than resting (non-reward) periods (Fig 1g, Extended Data Fig 4j; P=1.8e-4, Wilcoxon sign-rank test across all fields, n=6 mice). However, no significant difference in the fluorescence baseline (periods with no significant calcium transients) was found between locomotion and resting (Fig 1f; P=0.45, Wilcoxon sign-rank test across all fields, n=6 mice). Moreover, the duration of nearly all significant dopamine transients (n=2087) was far less than the duration of the average locomotion bout (mean locomotion bout 10.3+/−11.2s, Extended Data Fig 3e). Thus in dorsal striatum, treadmill locomotion is associated with widespread and synchronous sub-second transient increases in GCaMP6f fluorescence in dopamine axons, suggestive of phasic dopamine release, but is not associated with detectable long-duration transients or sustained changes in baseline fluorescence levels, suggesting little slowly-varying dopamine release.

Dopamine signaling to acceleration bursts

We first examined whether the widespread fluorescence transients in dorsal striatum displayed a timing preference with respect to locomotion initiations on the treadmill (sharp rest-run transitions; Fig 2a,d,f, Extended Data Fig 4a,b). On average and at individual onsets, GCaMP6f transients increased rapidly just prior (~100–150ms) to acceleration onsets occurring at locomotion initiation (Fig 2a, Extended Data Fig 4a,j,l,o; cross-correlation peak at −143+/−250ms std, significantly different from 0 lag, P =0.003, Wilcoxon sign-rank test across peak correlation times, Fig 2d,f). Thus, signaling across a widespread population of dopaminergic axons leads locomotion initiation in dorsal striatum, suggesting that sub-second dopamine signaling plays a role in initiating locomotion bouts.

We then examined whether the widespread fluorescence transients displayed a timing preference with respect to discrete phases of continuous mouse locomotion movements. Movements consisted of rhythmic acceleration bursts on the treadmill over a broad frequency range centered on ~2.5Hz (Extended Data Fig 4e). Indeed, fluorescence transients displayed a delayed timing preference with respect to acceleration bursts (Fig 2) during continuous locomotion (Fig 2b,e,f, Extended Data Fig 4c,d), where on average they *followed* the onsets (zero crossing) of individual acceleration bursts (Fig 2b,g; cross-correlation peak at 215+/−90 ms std, significantly different from 0 lag, P=1.66e-4, Wilcoxon sign-rank test across 18 fields, Fig 2e,f; Extended Data Fig 5a,b; n=6 mice), an effect which was also clearly observed with individual isolated transients (Extended Data Fig 4c,k). Importantly, the acceleration-associated calcium transients were observed *before* the mice ever received rewards on the treadmill (Extended Data Fig 4h,i), and the signaling was highly similar after the introduction of unpredicted rewards. Thus, contrary to current widely-accepted models,

these results establish the existence of a widespread population of dopaminergic axons projecting to dorsal striatum that display rapid phasic signaling associated with ongoing accelerations, which are expressed independently of reward expectation.

We then investigated whether the dopamine signaling during continuous locomotion might impact subsequent movements. We observed a significant correlation between calcium transient amplitudes and the amplitudes of the immediately *following* acceleration bursts (Spearman's Rho = 0.13, P = 0.006, all transient-acceleration pairs; binned data, Extended Data Fig 5d), despite a weaker temporal association (compared to previous acceleration bursts, Extended Data Fig 5a,b). Additionally, just prior to locomotion termination (stopping), calcium transient amplitudes associated with the last acceleration burst (before termination) were reduced compared to the transient amplitudes expected from similar acceleration bursts during continuous locomotion (Fig 2c, arrow). Thus, during continuous locomotion, dopamine axon transients appear to be more temporally associated with the previous (rather than following) acceleration burst (Fig 2b,e,f,g; Extended Data Fig 5a,b) and may positively impact the following acceleration burst (Extended Data Fig 5e), perhaps acting as a feedback signal to promote plasticity or continued locomotion.

Locomotion triggered by dopamine axon stimulation

To test whether sub-second timescale signaling in dopamine axons can trigger or alter locomotion, channelrhodopsin[35] (ChR2) was expressed in midbrain dopamine neurons of DAT-cre mice (n=7) and (bi-laterally) optically stimulated the dopamine axons in dorsal striatum (Fig 3a, Methods). Optical stimulation consisted of 166 or 83 ms duration bursts of 8 ms pulses (pulses repeated at 60Hz); these bursts were then repeated at 3 or 6 Hz, respectively (see Fig 3b; frequencies corresponding to rhythmic accelerations measured during average, 3 Hz, or fast, 6 Hz, locomotion--Extended Data Fig 4e) to create stimulation trains. This was intended to generate rapid phasic dopamine axon signaling similar to that observed during locomotion. The laser stimulation trains reliably trigged rapid transitions from resting to locomotion (or occasionally rocking forward and back; Fig 3c–g; statistically significant acceleration increase averaged across all mice and sessions, $p<0.01$, shuffle test; statistically significant increase in acceleration, averaged across all sessions for 6 out of 7 individual mice, $p<0.01$, shuffle test), though not every stimulation led to locomotion (Fig 3d,e). Transitions to locomotion were rapid: for 3Hz burst trains, acceleration significantly increased from rest after the first burst (i.e. ten 8-ms pulses; significantly increased acceleration compared to shuffle ~160 ms after burst onset, $p<0.01$; Fig 3g; similar to timing during spontaneous initiations, Fig 2a,d,f, Extended Data Fig 4l), while for 6 Hz burst trains, acceleration significantly increased from rest after two bursts (i.e. two bursts of five 8-ms pulses; significantly increased acceleration compared to shuffle ~240ms after burst onset, $p<0.01$; Fig 3g). Interestingly, 3 or 6 Hz stimulation trains that continued after locomotion initiation were capable of shifting the acceleration frequency in individual mice (Fig 3h) towards the stimulation frequency during the ensuing locomotion bout. All mice (n=7) displayed higher frequency accelerations during locomotion bouts initiated during 6Hz stimulation than during 3Hz stimulation (Fig 3i,k, significant shift, $p<0.01$, Wilcoxon Rank Sum test) despite equivalent mean velocities during these periods (Fig 3l). In two mice, acceleration power spectra peaks matched the respective stimulation frequencies (one of two

mice in Fig 3h, top) and accelerations during locomotion were significantly entrained to the laser stimulations ($p<0.01$, shuffle test; Extended Data Fig 6a,b; entrainment also significant across all mice, $P<0.01$ shuffle test, Extended Data Fig 6c,d). Critically, the same optical stimulation applied to control mice without ChR2 expression failed to trigger locomotion or shift or entrain locomotion frequency (n=7, Fig 3f,j,k, Extended Data Fig 6c,d). Thus, optogenetic stimulation of dorsal striatum projecting dopamine axons can trigger locomotion bouts and shift or entrain rhythmic acceleration frequency, demonstrating that signaling in dorsal striatal dopamine axons can impact locomotion movements on sub-second timescales.

Dopamine axon functional heterogeneity

Unpredicted rewards are well-known to trigger phasic bursts of dopamine signaling[6–9,13,18]. Surprisingly, we observed little or no phasic response to randomly delivered water rewards in the mean whole-field DF/F traces; instead the signals decreased in accordance with the deceleration from locomotion to reward consumption or remained flat when reward was delivered at rest (Extended Data Fig 4f,g). However, a small, sparse population of axons were found which signaled during reward (Fig 4a). To characterize reward and locomotion signaling at the individual axon level, we then sparsely labeled small populations of midbrain dopamine neurons (Fig 4b, Extended Data Fig 7), resulting in sparse labeling of axons in dorsal striatum. This enabled us to resolve the fluorescence changes from putative single axons (Fig 4c,d; Extended Data Fig 8a,b) and revealed that, as suggested by the widespread labeling experiments (Fig 4a), putative single axons in the same dorsal striatum region can differentially signal unpredicted reward and locomotion (Fig 4d–i). Thus, the dopaminergic projection to dorsal striatum is heterogeneous with respect to unpredicted reward and locomotion, but is dominated by locomotion signaling.

We then examined whether these functionally distinct axons emanate from different midbrain nuclei[36]. Injections were localized primarily to either SNc (n=5 mice) or medial VTA (n=5 mice) (Extended Data Fig 7). 73 isolated putative single axons (Methods) were imaged from SNc and 98 from VTA, of which 63/73 (86%) and 72/98 (73%) respectively responded to locomotion and/or reward events ($P<0.01$, Wilcoxon rank-sum test, locomotion vs rest; during unpredicted reward delivery, $P<0.01$, shuffle test vs non-reward periods; or during both). The large majority of the responsive VTA axons signaled unpredicted reward (Fig 4k,l,n; 53/72 axons, 74% reward responsive). These responses were consistent with documented single-unit electrophysiology and FSCV[5,8–10,18,37]: they were absent on omission trials, scaled with reward-size, were not present to licking in the absence of reward, and were present whether reward was delivered during running or rest (Extended Data Fig 9). In contrast to the VTA, such prominent reward signaling was absent from active dopamine axons emanating from SNc (Fig 4k,l,n, Extended Data Fig 9; 0/63 axons). Instead, all event responsive axons from SNc displayed significantly increased signaling during locomotion compared to rest (Fig 4n; 63/63 axons). This signaling was transient rather than sustained (Fig 4j,m, Extended Data Fig 2g,h) and displayed a timing preference with respect to acceleration similar to the whole-field measurements (Fig 2a–g), indicating that single SNc axons, rather than different subpopulations, can signal during locomotion initiation and continuous locomotion (Extended Data Fig 8c–e). Only a minority of the total responsive VTA (Fig 4k,m–o; 29/72 axons, 40%) and reward signaling VTA (Fig 4m–o; 10/53 axons,

19%) axons significantly increased signaling during locomotion compared to rest, but similar to the SNc projections, this signaling was transient and acceleration-associated. Overall, reward and locomotion signaling were negatively correlated in the heterogeneous VTA axon population (Fig 4n; Rho=−0.51, P=5.7e-6). The presence of both reward and locomotion signaling axons from the VTA likely reflects some within-region heterogeneity, however some expression spillover into SNc[36] or SNc/VTA border region may contribute to the locomotion population. Taken together, these results demonstrate a previously unknown functional heterogeneity within dorsal striatum projecting dopamine axons, which, for the most part, arise from different anatomical nuclei: sparsely projecting reward signaling axons originate primarily from VTA while densely projecting SNc originating axons generate an acceleration-associated locomotion-signal.

Dopamine signaling functional topography

Due to the prominence of unpredicted reward signaling in previous recordings[4,7,9,17,19,37–39], the small fraction of reward signaling dopamine axons in dorsal striatum was surprising. However, because ventral striatum receives the majority of its dopaminergic innervation from VTA, while dorsal striatum receives the majority from SNc[36], we reasoned that locomotion and unpredicted reward signaling might be similarly graded across the striatum. Single-photon photometry[34,39] was used to record from the GCaMP6f expressing dopamine axons along the dorsal-ventral axis (Fig 5a; n=5 mice). This method lacked single axon resolution, but provided a means of recording throughout the striatum with minimal tissue damage. Recordings from dorsal striatum revealed acceleration-associated dopamine signaling highly similar to that observed with two-photon imaging (Fig 1e, 2e–k vs. Fig 5b–d, Extended Data Fig 10a–f; serving as a control for the cortical lesion required for two-photon imaging). More ventrally, acceleration-associated signaling declined while unpredicted reward signaling increased (locomotion index vs depth, Rho=0.7, P=6e-6; reward signal vs. depth: Rho=−0.65, P=5.2e-5; Fig 5c,d, Extended Data Fig 10g) and dominated in ventral striatum (Fig 5c,d, Extended Data Fig 10g). Consistent with this result, pulsed optogenetic stimulation of dopamine axons in ventral striatum had comparatively little effect on locomotion (Extended Data Fig 6e–h; n=4 mice, same ChR2 expressing mice as used in Fig 3). No significant dopamine signaling was seen in the overlying sensory cortex (Fig 5c,d). Thus, a functional topography in dopamine signaling exists across the striatal dorsal-ventral axis[34], with locomotion and reward signaling dominating dorsal and ventral striatum, respectively.

Discussion

The rapid, phasic, acceleration-associated locomotion signaling of dopamine projection axons described here represent a novel mode of dopaminergic modulation of striatal circuitry and establish strong evidence for the long-elusive role for dopamine neurons in fast-timescale motor-control. This result is perhaps surprising given the little evidence for movement-related dopamine signaling previously observed; this difference may be due to task and/or methodological differences (Supplemental Discussion). Our results support new models of dopaminergic signaling that incorporate rapid, sub-second modulation of movement by dopamine[16,20,21] over current models that posit a permissive involvement by a

slowly varying background[12,14,15,40] (Extended Data Fig 10h–k). The phasic signaling occurred in the absence of action requirements or rewards, suggesting a general role in internally driven movement control.

Our optogenetic stimulation experiments support the idea that the phasic signaling in dopamine axons observed with optical recording can trigger and entrain locomotion movements on a sub-second timescale, demonstrating the utility of using measurements of natural neuronal dynamics[41] to define stimulation[35] parameters for effecting a desired behavioral outcome[42]. Dopamine signaling is part of a complex circuit regulating voluntary movement, and therefore is unlikely to instruct movement alone. The behavioral effects of these signals may therefore be strongly modulatory, rather than deterministic, an idea supported by the variability in signaling timing and stimulation effects on locomotion (Fig 3d,h–k, Extended Data Fig 4j,k), though this could also be partly due to the limited region imaged or stimulated. Dopamine signaling could interact differently with the many converging components of the movement network during movement initiations versus continuous movements. At initiations (Fig 2a,d,f, Extended Data Fig 4a,b,j), dopamine may provide the necessary motivational drive to execute an intended movement. During ongoing movements, dopamine signaling lagging behind accelerations (Fig 2b,e,f,g, Extended Data Fig 4c,d) may modulate upcoming movements (Extended Data Fig 5d,e), determine whether dorsal striatum circuitry maintains an existing motor pattern (Fig 2c, Extended Data Fig 5e), or instruct motor learning. Importantly, these findings establish a movement signal that is likely compromised in Parkinson's disease, and suggests the potential therapeutic utility of restoring precisely-timed, movement-associated dorsal striatum dopamine signaling[43].

Finally, distinct populations of axons signaling to reward or locomotion were observed both locally within dorsal striatum and globally across the striatum's dorsal-ventral axis suggesting regional tuning to regulate the specific functions of the terminal regions[34,39]. Heterogeneity of midbrain dopamine neurons has been described in terms of inputs[44,45], gene expression[46–48] and electrophysiological properties[47,49]; such cellular heterogeneity may align with the functional subpopulations described here (Supplemental Discussion)[39,44,45,50]. Specific targeting of these populations, and the local mechanisms such as cholinergic modulation[23,24] that shape their signaling, may provide novel therapeutic opportunities for neurological disorders.

Methods

Virus Injections for Optical Recording

All experiments were approved by the Northwestern University Animal Care and Use Committee. Heterozygous adult male mice (postnatal 3–4 months) with Cre expression in DAT containing midbrain dopamine neurons (GENSAT line Tg(Slc6a3-cre)SG62Gsat/Mmucd) were anesthetized with isofluorane (1–2%). For achieving widespread expression of GCaMP6f in dopaminergic neurons (n = 6, Figs 1, 2, 4a, 5, Extended Data Figs 1, 2k, 3e, 4, 5, 10), a 0.5–1mm diameter craniotomy was made over the right midbrain (−3.4mm caudal, +1.0 lateral from bregma). A small volume (0.04ul) of flexed–GCaMP6f virus (AAV1–Syn–flex–GCaMP6f, 1.4×10^{13} GC ml^{-1} diluted 1:1 in PBS; University of Pennsylvania vector core) was pressure injected through a pulled glass micropipette into the

midbrain at two caudal locations (~−3.3 and −3.5mm from bregma) and 3 depths at each location (−4.1, −4.4, and −4.7mm ventral from dura surface) for a total volume of ~0.24μl. For sparse, targeted injections (Fig 4b–o, Extended Data Figs 2, 3, 7, 9, 8), the craniotomy was centered over either the medial VTA (n = 3; caudal −3.1mm, lateral 0.2mm) or lateral SNc (n = 5; caudal −3.4mm, lateral 1.5mm) and virus (0.025 μl – 0.05 μl) was injected at two ventral locations (−4.3, −4.6mm) for a total of ~0.08μl. Following the injections, the skull and craniotomy were sealed with Metabond (Parkell) and a custom metal headplate.

Dorsal Striatum Window Implant Surgery

One week post-injection, mice were again anesthetized, and the headplate and metabond removed. A ~2.75mm craniotomy was performed above the dorsal striatum (+0.5mm rostral, +1.8–2.1mm lateral to bregma) and cortical tissue was aspirated until the internal capsule fibers overlying the striatum were exposed[1]. Some of these fibers were then carefully removed until only a thin layer remained over the striatal surface. A thin (~100μm) layer of Kwik-Sil (WPI) was applied over the imaging region, and a metal cannula (stainless-steel tube, 2.7mm outer diameter, 2.3 mm inner diameter, 1.6mm length) covered at one end by a glass coverslip[1] was inserted into the aspiration site down to the fiber surface (Extended Data Fig 2i). The imaging cannula, along with a metal headplate, and positioning ring (see[1] for details) were sealed and attached to the skull with Metabond.

Behavior and 2-Photon Imaging

After the window surgery, the mice were allowed to recover in their home cages for ~2–3 days. After this time, the mice began water scheduling (receiving ~0.8–1mL of water/day) as described previously[1,2]. The mice displayed no obvious signs of motor deficits following window implantation or water scheduling. After 3–4 weeks post-implant surgery, mice were head-fixed with their limbs resting on a 1D cylindrical styrofoam treadmill ~8in in diameter by 5in wide (treadmill described previously[3], Fig 1b) in the dark, which allowed them to run freely forwards and backwards. Large (16μL) and small volume (4μL) water rewards were delivered at pseudo-random time intervals (mean 28.1s +/−19.8s std) through a water spout gated electronically through a solenoid valve once imaging began, and spout licking was measured by a contact monitoring circuit. Solenoid valve triggering was accompanied by a short “click” noise, which allowed us to conduct reward omission trials in which the water tube was manually closed (Extended Data Fig 9a,b). Rotational velocity of the treadmill during locomotion was sampled at 1000Hz by a rotary encoder (E2-5000, US Digital used for most experiments; a few early experiments used a E6B2-CWZ3E, Yumo) attached to the axel of the treadmill. Instantaneous acceleration was calculated as the difference between consecutive treadmill velocity (first smoothed over 2 bins) measurements. Live video of behavior on the treadmill was recorded at 30Hz via a table mounted infared CCD camera (Computa) illuminated by an infared light source.

Two-photon imaging was performed using a custom, table mounted microscope system and data acquisition system described in[4] (except the electric lens was not used here). Laser (920 nm) average power was in the range of 100–200 mW, but typically closer to 100mW: This power measurement was made after the objective (Olympus LUMPlanFL N, 40X,0.8 NA), but before the cannula, which apertures the excitation light, likely further reducing the power

reaching the striatum. A Digidata1440A (Molecular Devices) data acquisition system was used to record (Clampex 10.3) and synchronize reward timing, licking, wheel velocity, and two-photon image frame timing. Imaging sessions began after mice were acclimated to head fixation and ran frequently on the treadmill (~1–3 days). To rule out the influence of prior reward experience on locomotion responses, a subset of mice (n = 4) were imaged prior to receiving any water rewards on the wheel (Extended Data Fig 4h,i). Time series movies (3,000–12,000 frames) were acquired at 28Hz (256 × 64 pixels, 0.5ms/line). A subset of the sparsely-labeled single axon recordings were performed at 14Hz (256 × 128 pixels, 0.5ms/line) to achieve better spatial resolution for resolving small axonal arbors. For triggered averages (Fig 4j,k,m), DF/F fluorescence traces generated from these 14Hz imaging datasets were linearly interpolated to match the data collected at the 28Hz sampling rates. Field of view sizes ranged from ~60um to ~250μm.

Striatum imaging fields (60–250μm diameter fields) were selected based on the presence of fiber morphology with at least occasional calcium transients in the fibers (field were not selected based on the behavioral correlation of the transients, only whether transients were clearly present) and, for widespread dopamine neuron expression experiments (Figs 1–2, Extended Data Figs 1,3,4,5), densely labeled projections across the field, or for sparse dopamine neuron expression experiments (Fig 4, Extended Data Figs 7,8,9), few labeled projections in the field. Fields ranged in depth from 20–100 μm below the fiber surface. Each mouse was imaged for ~5–10 days, with multiple fields imaged per day (an “imaging session” consisted of time-series recording from a single field, typically for many minutes); ~5–15 total different fields were imaged per mouse across all days (not all sessions met behavior criteria to be included in all analyses, see below); no attempt was made to locate the same imaging field/axons from day to day, except in a small subset of experiments to demonstrate that axon morphology and behavioral signaling remains stable over days (Extended Data Fig 2). Imaging up to ~700um from the center of the cannula was possible, though most fields were acquired near the center of the cannula. Thus, the majority of our imaging fields were located more laterally in the dorsal striatum (~1.5mm–2.4mm lateral from the midline), but some medial fields were obtained as well (most medial, ~1.1mm from midline, Extended Data Fig 1). Imaging along the rostral-caudal axis ranged from −0.2mm to 1.2mm from Bregma. There was no preference for recording location within this large range of positions and no obvious differences in dopamine signaling were observed within this range.

Interpretation of mechanisms underlying calcium transients and characterization of putative single dopamine axon calcium transients

The time-course of fluorescence changes caused by changes in cytoplasmic calcium concentration are well-known and characterized[5,6], providing a significant framework within which to interpret our observed calcium transients (Extended Data Fig 3a–c). For example, a short tens of milliseconds timescale influx of calcium (e.g. short burst of action potentials over tens of milliseconds) results in a stereotyped calcium transient consisting of a fluorescence increase to peak over ~50–70ms followed by an exponential decay to baseline over ~150–250ms (Extended Data Fig 3a). Multiple influx events separated by less than the indicator decay time (e.g. longer bursts of action potential firing over ~100’s of

milliseconds) lead to longer duration, larger amplitude calcium transients due to summation (Extended Data Fig 3b), while a sustained increase in the rate of influx events separated by less than the decay time (e.g. sustained increase in action potential firing) leads to sustained elevations or apparent shifts in the fluorescence baseline due to ongoing summation[7] (Extended Data Fig 3c left). Thus, GCaMP6f fluorescence changes are well-suited for determining whether mouse locomotion (accelerations on the 100s of millisecond timescale) is associated with sub-second phasic dopamine signaling (rapid transient changes in fluorescence), slowly varying dopamine signaling (long-duration transients or changes in the GCaMP6f baseline level over many seconds or minutes) or both. However, our imaging methods likely cannot reliably detect single action potentials in single axons, or the difference in transient amplitude due to an additional spike in a burst. Furthermore, it is possible that small, slow changes in action potential firing could occur between rest and locomotion and not be detected using our optical recording methods. Also, although we did not detect slow changes in signaling here, such changes could occur over timescales longer than our typical recording sessions (many minutes).

Optical stimulation of dopamine axons

To achieve wide-spread expression of ChR2 in dopaminergic axons in striatum, DAT-cre mice (n = 7; 5 male, 2 female; postnatal 3–6 months) were injected bilaterally (0.2 – 0.3μL total per hemisphere) as above with AAV9-EF1a-DIO-hChR2 (University of Pennsylvania vector core diluted 3:1 in PBS to 3.5×10^{12} GC/mL) in the midbrain (−3.3mm caudal, +/−1.3mm lateral from bregma) at three depths (−4.1, −4.4, −4.7mm from the dura surface). Headplates for head fixation were then attached to the skull with a thin layer of Metabond and the location of the striatum (+0.5mm rostral, +/−1.8mm lateral from bregma) was marked on the surface. After 4–6 weeks[8], mice were anesthetized with isoflourane and small craniotomies (~0.5–1mm in diameter) were drilled (at the pre-marked locations) through the Metabond and skull over the striatum, leaving the dura and cortex intact. The craniotomy was then sealed with Kwik-Sil. After the mice recovered from this short (~10–15 min) surgery for at least one day, they were head-fixed on the linear treadmill. When mice began to exhibit periodic, spontaneous run-rest transitions on the treadmill, the Kwik-Sil covering the craniotomies was removed and two optical fibers (200μm diameter, ThorLabs) were lowered slowly into the brain bilaterally (to various depths ranging from dorsal: 1.6–2.2mm to ventral striatum 3.6 to 4.1mm) to allow for delivery of laser light (488nm diode laser, Thor Labs). Laser stimulation (5mW laser power at the fiber tip) trains consisted of 83 ms ON/83 ms OFF (6 Hz) or 166 ms ON/166 ms OFF (3 Hz) periods and the laser was pulsed (8ms ON/8ms OFF, using an optical chopper, ThorLabs) during the 83 or 166 ms ON periods. We refer to this stimulation as a train of 8ms pulse bursts repeated at 3 or 6 Hz. For example, for 6 Hz stimulation, the laser stimulation trains consisted of the following: 8ms ON/8ms OFF/8ms ON/8ms OFF (repeated for 83ms) followed by 83ms with no stimulation and then the whole sequence repeated (Fig 3b). The onset of laser stimulation trains were triggered manually via a pulse generator and synchronized to output from the treadmill rotary encoder through our data acquisition system (see above). Stimulation trains (mean duration 8.6s+/−2.8s std) were initiated periodically at pseudorandom intervals primarily during rest periods during 1–8 stimulation blocks (sessions) per mouse per day at varying depths in striatum (3–5 min block durations, all occurring during a single ~40 min recording

period on the treadmill per day per mouse). Importantly, bright LED lights (470nM and 530nM ThorLabs) provided constant illumination onto the face of the mice on the treadmill during the stimulation blocks to mask the mice from the fiber optic light delivered to their brain. After stimulation was completed, craniotomies were again covered with Kwik Seal to allow for additional sessions on subsequent days (1–3 days/mouse). We note that effects highly similar to those shown in Fig 3 and Extended Data Fig 6a–d were obtained using the above laser stimulation trains, but with either faster pulsing (4ms ON/4ms OFF) during the 83 or 166 ms ON periods or no pulsing at all (only 83 ms ON/83 ms OFF, 6 Hz or 166 ms ON/166 ms OFF, 3 Hz); however all data presented in the manuscript were obtained using the 8ms pulsing during bursts protocol.

Single Fiber Photometry

For fiber photometry we coupled the blue diode laser excitation light (488nm diode laser, Thor Labs; filtered using a 488/6nm filter, Semrock) into an optical fiber (200μm diameter, ThorLabs) and used neutral density filters between the laser and fiber coupling lens to adjust power (1mW at fiber tip). Fluorescence was collected through the same fiber and was separated from the excitation light by placing a dichroic mirror (505nm-shortpass, Semrock) between the laser and fiber coupling lens. Fluorescence light was further filtered (540/50nm, Semrock) and then measured using a GaAsP PMT (H10770PA-40, Hamamatsu). The PMT signal was digitized and recorded using the electronics and ScanImage software from our two-photon microscope (described above). Synchronization of the recorded fluorescence with treadmill movements was accomplished as described above for two-photon imaging.

DAT-cre mice (n = 5) were injected with viral vectors to obtain ubiquitous GCaMP6f expression in midbrain dopamine neurons as described above for 2-photon imaging experiments and fitted with plates for head-fixation as described for the ChR2 experiments. At 3–5 weeks post injection, mice were trained for 1–3 days on the linear treadmill with rewards until they ran reliably. Mice were then anesthetized with isoflourane and a unilateral craniotomy (~0.5–1mm in diameter, dura and cortex were left intact) over the central striatum (+0.5A/P, +1.3–1.8mm M/L from bregma) was performed. After the short (~10–15 min) surgery, mice were head-fixed on the linear treadmill. When mice began to run regularly on the treadmill, the optical fiber was lowered slowly into the brain to various depths ranging from Cortex to Ventral Striatum for photometry recording (Fig 5, Extended Data Fig 10). Unpredicted rewards were delivered as described above.

Data Analysis

Data were analyzed using ImageJ (1.46) and custom functions written in MATLAB (Version 2012b). Sample sizes were chosen to reliably measure experimental parameters while remaining in compliance with ethical guidelines to minimize the number of animals used. Experiments did not involve blinding, but randomization was used with respect to reward delivery and order of data collection from control vs. experimental mice. All data in the text and figures are labeled as either mean ± s.d. or mean ± s.e.m.

Motion Correction and ROI Selection for two-photon microscopy—Each time series movie was motion corrected using algorithms described previously[1,9]. Movies were

then visibly inspected to confirm post-correction image stability and movies with excessive motion artifact or apparent z-shifts were excluded from analysis. To quantify whole-field fluorescence (Figs 1–2, Extended Data Fig 1,2k,3e,4,5) a single large region of interest (ROI) was hand selected (to contain all the active regions of the field) from the mean fluorescence image for each time series. Fluorescence traces and ROIs from putative single axon segments from the sparsely labeled fields (Fig 4, Extended Data Figs 7–9) were generated using CellSort[10] with the following parameters: smoothing width = 1.5, mu = 0.8, principal components = 200, area limits = 50 – 3000 pixels. ROI fluorescence traces and ROI morphology were visibly inspected and selected for inclusion as a putative axon if they exhibited elongated morphology consistent with axons (Fig 4c) and activity patterns with predominantly positive-going fluorescence changes (no structures with slowly varying fluorescence activity patterns were observed). The fluorescence traces were then baseline normalized (8^{th} percentile fluorescence over a 1000 bin, ~35.7s, sliding window, to remove any slow drifts in baseline; see below for measurements of slow changes in baseline) and converted to DF/F. Significant positive-going transients (used for Figs 1g, 2g, 4k–o; Extended Data Figs 2g–h, 3d–e, 4h,i (bottom), 5a–b, 7, 8, 9, and 10a–c) were identified as previously described[1]. To account for axon segments which likely originated from the same neuron, hierarchical clustering (simple linkage) of the linear correlation matrix between DF/F traces of all segments in each field was performed using a correlation coefficient threshold of 0.8 (results were similar using other clustering thresholds, Extended Data Fig 8a,b), and DF/F traces belonging to the same cluster were averaged. To verify single axon separation from background, analysis was run only on the most sparsely expressing fields; separation of functional axon classes was qualitatively similar to Fig 4n using this more conservative approach (Data not shown).

Relationship of fluorescence signals to treadmill locomotion—All mice (n = 6 whole field, n = 5 for each single-axon imaging group, n = 5 for photometry) contributed to averaged measures unless otherwise noted in the text or figure captions. Individual imaging sessions were excluded if they did not meet criteria for each specific behavioral analysis (i.e. locomotion initiation, continuous locomotion, locomotion terminations; see below for each), hence the session "n's" varied slightly for each measure. For general comparisons of fluorescence changes in whole fields and single axons during locomotion and rest periods (Figs 1f–g, 4n–o; Extended Data Figs 2f, 4h, 7, 8,10a–c,g), we classified each imaging frame (~35ms bin size) as occurring during active locomotion, passive rest, or neither (uncertain, excluded). All bins occurring within 5.5s post-reward delivery or during a spontaneous licking period were excluded. Locomotion bins were identified as those that had a treadmill velocity measure greater than 0.2 m/s and an acceleration greater than 1.7 m/s^2 in a 200ms window on either side. Conversely, rest bins were defined as having no accelerations greater than 0.3 m/s^2 or velocities greater than 0.05 m/s. These parameters were determined based upon visual comparison of live video with acceleration and velocity traces and are likely conservative constraints. To be included for locomotion/rest comparisons, behavior over the entire imaging session had to include a minimum of 30 rest bins and 30 locomotion bins. Slow, sustained changes in baseline fluorescence (Figs 1f and Extended Data Fig 10a–c) were quantified by comparing DF/F for locomotion and resting periods that did not contain significant calcium transients. The DF/F baseline normalization

was re-computed for this calculation using a larger sliding window (2000 bins, ~70.4s) to ensure that slow events over multiple locomotion bouts (Extended Data Fig 3e) would be detected if they were present. Further, examination of DF/F traces with no baseline normalization did not reveal slow events corresponding to locomotion bouts (Extended Data Fig 2k).

Locomotion initiation times for triggered averages of fluorescence (Figs 2a,d,f and 4h, Extended Data Fig 4a,b; Extended Data Figs 4j and 10d–f) were first identified manually by visual inspection of velocity traces for each session. Typically, mice exhibited clear transitions between rest (periods with few treadmill accelerations) and continuous treadmill locomotion. Bursts of acceleration not followed by a prolonged elevation in velocity (indicative of continuous locomotion) were not selected. Manually selected initiations were included for analyses only if they were followed (within 10 bins, ~350ms) by an acceleration peak greater than 1 m/s^2 and were not preceded within 1s by any velocity bins larger than 0.05m/s or accelerations larger than 0.3m/s^2. Acceleration-triggered averages were calculated relative to the onset of the first acceleration (after the manually defined time point) greater than 0.3m/s^2. Locomotion terminations (Fig 2c) were also selected manually as the first deceleration to rest following locomotion bouts. One termination time-point was selected for each initiation. Terminations were included if they were preceded (within 10 bins) by a maximum velocity greater than 0.1 m/s, indicating a sharp locomotion to rest transition. For defining periods of acceleration occurring during continuous running (Figs 2b,e,f, Extended Data Fig 4c,d,k,m and 8d–e), accelerations were required to be preceded (within a ~200ms window) by a minimum run velocity of (0.1m/s) and followed by a mean run velocity (over 200ms) of 0.1m/s. Non behavior-specific acceleration triggered averages of fluorescence (Fig 4j,m, 5d and Extended Data Fig 4i, top) were calculated for all accelerations exceeding 1.7m/s^2 (i.e. accelerations occurring during continuous locomotion, locomotion onsets and any other short movements not falling into either of these two categories, though the vast majority occurred during continuous locomotion).

For acceleration triggered averages of DF/F, single average DF/F traces were derived for each field (Figs 1 and 2), putative single axon (Fig 4), or photometry recording location (Fig 5, Extended Data Fig 10) across all identified accelerations (meeting acceleration criteria, triggered on the zero crossing of the acceleration trace when the acceleration was increasing and crossed a threshold value >1.7m/s^2) in an imaging session; and these traces were averaged across sessions and mice to generate summary traces. DF/F triggered averages of acceleration were calculated analogously (Fig 2g, Extended Data Fig 4i, bottom, triggered on the onsets of significant, positive-going DF/F transients). For these traces, and for analysis of amplitudes of preceding and following accelerations bursts (Extended Data Fig 5c,d) only significant transients <0.5s duration were included to avoid inclusion of any sustained summated transients. Shuffled triggered averages were computed relative to an equivalent number of randomly selected time-points (randsample in MATLAB). Correlations (Pearson's) between acceleration and DF/F were calculated between the (concatenated) traces around all initiation bins (+/−750ms around each) or continuous locomotion periods (+2s after locomotion initiation to locomotion termination). Note that differences in the criteria for selecting different behavior periods (locomotion initiations,

terminations, continuous running periods, etc) results in the inclusion of a different number of fields or axons for each behavior (i.e. Fig 2a–e).

Single-photon fiber photometry fluorescence data was first averaged over 35.7ms bins and then corrected for background signal (intrinsic fluorescence and laser bleed-through). The signal recorded in the unlabeled cortex (estimated in a subset of the recordings) was assumed to be background and this signal was subtracted from the striatum signal. After this subtraction, the remaining photometry signal (assumed to be GCaMP6f fluorescence) was analyzed identically to the whole field two-photon imaging datasets described above.

Relationship of acceleration to ChR2 axon stimulation—Significant effects of laser stimulation on locomotion initiations (Fig 3d–g) were assessed by comparing the mean absolute value of acceleration within a 0.5–2s window (for each mouse and across all mice, Fig 3f) or for each bin (Fig 3g) following stimulation train onsets that were delivered during rest (no large accelerations within 2s prior to stimulation) across all mice and stimulation trains to the means obtained from 1000 rounds of randomly selecting an equivalent number of non-laser stimulation rest periods from the same stimulation sessions. Sessions were included if mice exhibited spontaneous locomotion/rest transitions in the absence of stimulation and exhibited average resting bout durations of >6s (to allow comparison with spontaneous transitions from rest to running). Stimulation effects were considered significant if the post-stimulation means were greater than 990 of the 1000 randomly selected means ($p < 0.01$). Note that because we analyzed laser train onsets that were preceded by 2s of rest, there was a slightly higher probability for mice to be moving in a window after the stimulation onset simply by chance. This explains the apparent small change in the control group (Fig 3f) at laser train onset and in the shuffle group (Fig 3g). A similar test was applied to assessing significant frequency dependent acceleration entraiment (Extended Data Fig 6c,d): Laser pulse triggered averages of acceleration were computed during locomotion periods beginning after laser train onset and the mean of absolute value of these triggered averages were compared with 1000 averages from randomly selected non-laser stimulation locomotion periods. Consistent phase relationships between the laser stimulation and acceleration produce significant positive and negative peaks in the triggered average (Extended Data Fig 6c,d), whereas traces with no consistent phase relationship result in flat triggered averages (see controls, Extended Data Fig 6c,d). Multi-taper power spectral densities of acceleration (Fig 3h) were constructed for all locomotion periods (minimum 3s of locomotion per stimulation train period) during 6Hz and 3Hz stimulation periods in each block using the *mtspectrumc* function in the Chronux library (http://chronux.org/) with 5 tapers and a time bandwidth product of 3 over the interval 1Hz to 8Hz. Power spectra across blocks were averaged to produce mean power spectra for each mouse (one each for 6 and 3Hz stimulations, Fig 3h). The center of mass (Fig 3i–l, Extended Data Fig 6f–h) was calculated from the top 25% of the mean power spectra for each mouse (though highly similar results were obtained using the top 50%, 75% or all of the power spectra).

Classification of functional signaling related to reward and locomotion across putative single axons and striatum locations—Axon heterogeneity in single fields

relative to reward and locomotion periods (Figs 4a and i) was visualized by computing the mean fluorescence image during locomotion bins (see above) and subtracting the mean fluorescence image during reward delivery (a 750ms window following reward delivery). Locomotion Index (Figs 4n, and Extended Data Figs 7,8,10g) was the difference between the mean DF/F during locomotion and rest ($D/DF_{move} - D/DF_{rest}$) and axons were classified as significantly locomotion responsive via a Wilcoxon Rank Sum Test ($p < 0.05$) between all locomotion and rest DF/F values. Reward responses (Figs 4n, and Extended Data Figs 7,8,10g) were defined as the mean DF/F in a 300ms window after reward delivery. Significance of reward responses were computed with a bootstrap test ($p < 0.05$) where the p value was the probability of receiving an equivalent or larger mean value from 1000 rounds of randomly selecting a trigger bin from all non-reward bins.

ROC analysis—ROC (receiver operating characteristic) curves (Extended Data Fig 4n,o) to assess the ability of calcium transients to discriminate locomotion from rest were computed using the “perfcurve” function in MATLAB for all bins for each imaging field that were classified as locomotion or rest based on the criteria defined above. The positive state was defined as locomotion, the negative as rest (Extended Data Fig 4n). For the onset ROC analysis to assess ability of calcium transients to discriminate pre-locomotor from other rest periods (Extended Data Fig 4o), all resting bins were classified as either being pre-onset (positive state, within 250ms prior to defined onset – see above) or non-pre onset (negative state).

Histology

Mice with injections targeting SNc or VTA (see above) were perfused trans-cardially with 15mL of PBS (Fischer) and 15mL of 4% paraformaldehyde (EMS). Brains were stored in PBS at 4 °C then transferred to 40% sucrose (Fischer) overnight before sectioning. Coronal slices (40–50μm) were cut on a freezing microtome and stored at 4 °C in PBS. For immunostaining of dopaminergic neurons, sections from a subset of mice were blocked in 5% serum, incubated overnight at 4 °C with antibodies for tyrosine hydroxylase (TH, 1:700 dilution, Millipore catalog #: AB152, Extended Data Fig 7), then incubated with secondary antibodies tagged with Alexa Fluor 594 (Jackson). Large area imaging of TH and GCaMP6f expression was performed on an Olympus Slide Scanner (VS120) microscope, and high magnification imaging of co-labeling (Fig 1d, right) was performed with a confocal microscope.

Extended Data

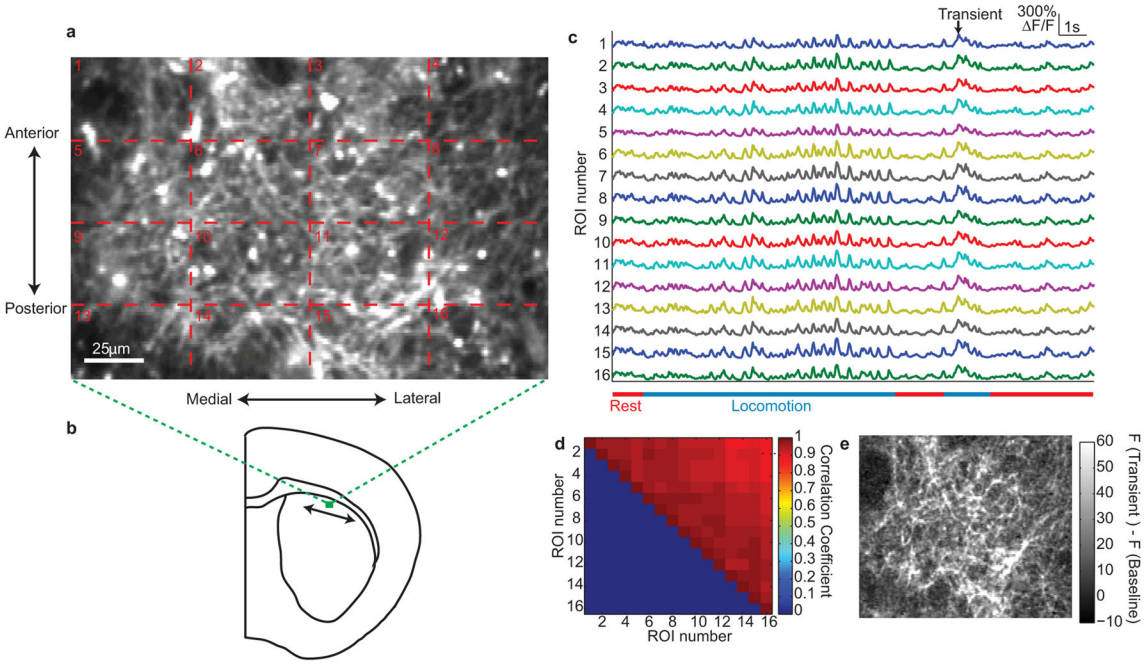

Extended Data Fig 1. Synchronized dopamine projection axon dynamics across a single field in dorsal striatum

a, Representative mean fluorescence image in dorsal striatum of a dense field of dopamine axons (compare to the sparse fields from sparse labeling, i.e. Fig 4c, i) from one mouse (out of 6) labeled with GCaMP6f. **b,** Coronal schematic showing approximate location and scale of region imaged at top. Arrow indicates the approximate range of medial/lateral positions used for two-photon imaging (see Methods). **c,** DF/F traces for the rectangular ROIs indicated in **a. d,** Correlation matrix for the ROIs indicated in **a**. Note high degree of transient co-activation across ROIs. **e,** Mean image of fluorescence during the transient indicated by the arrow in **c** minus mean image of fluorescence during non-transient periods for the field shown in **a**. Note that the morphology of active regions closely resembles the morphology of GCaMP6f expressing axons in the whole field in **a**, indicating synchronous activation of large, dense regions of axons, likely belonging to several different parent neurons.

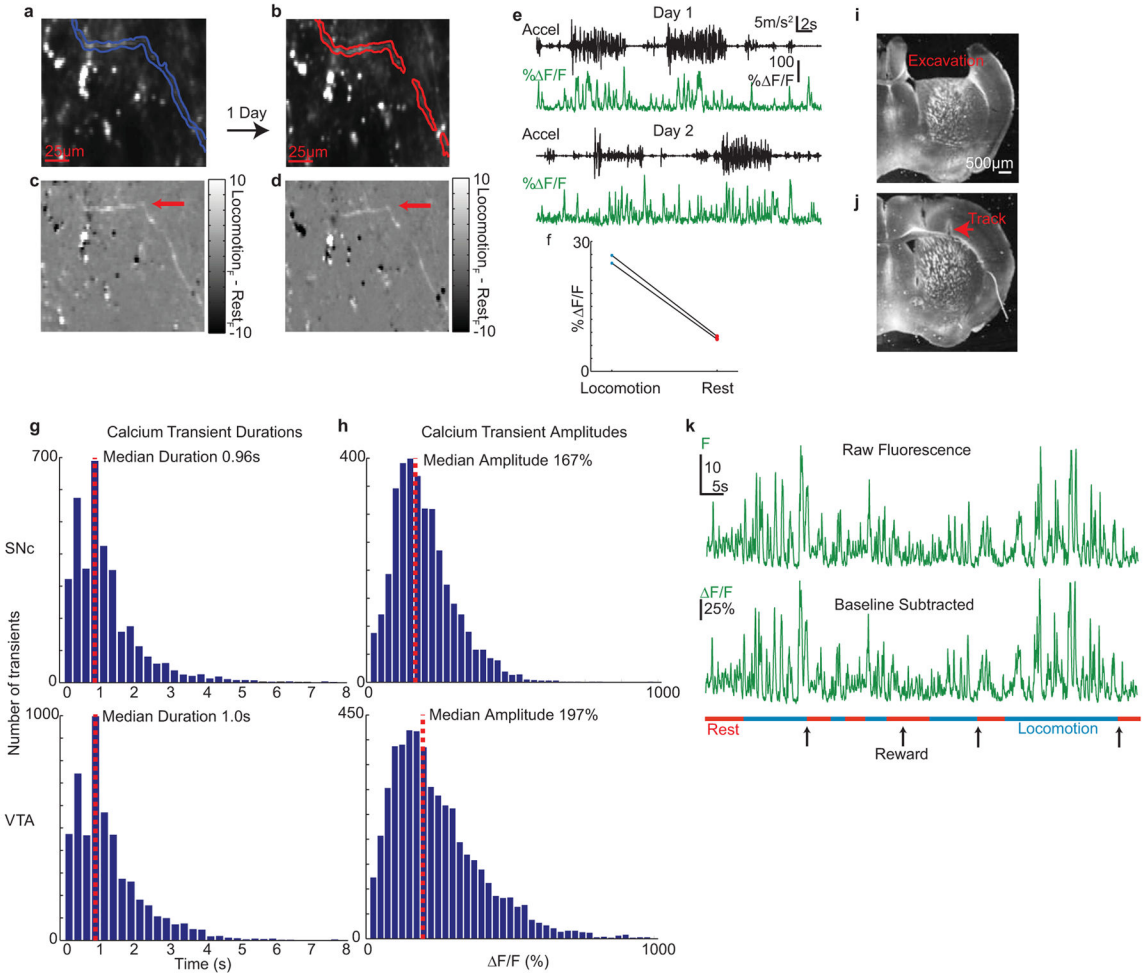

Extended Data Fig 2. Further characterization of two-photon imaging and analysis methods

a and b, Top, Example mean fluorescence images of a putative single SNc axon imaged over 2 consecutive days in one mouse. **c and d,** Mean images of fluorescence during locomotion periods minus mean image of fluorescence during reward periods for fields in **a and b**. White axonal regions indicate regions of elevated signaling during locomotion. Note the similar morphology and behavior signaling of the identified axon (red arrow) over days. **e,** Acceleration (black) and DF/F (green) for the identified axon in **a–d** across the two imaging days. Note the similar transient amplitudes and the elevated transient signaling during locomotion acceleration periods. **f,** Mean transient DF/F (mean of significant transients, excluding baseline periods) during locomotion and rest on days 1 and 2 for the axon shown in **a–d. g,** Histograms of calcium transient duration times across all putative single axons imaged in dorsal striatum from SNc (n = 3556 transients, 5 mice top) and VTA (n = 5140 transients, 5 mice bottom). Note the similar duration profile across the two populations (medians not significantly different, $P > 0.05$ Wilcoxon sign rank test). **h,** Histograms of maximum calcium transient amplitudes across all putative single axons imaged in dorsal striatum from SNc (top) and VTA (bottom) (medians not significantly different, $P > 0.05$ Wilcoxon sign rank test). **i,** Post-mortem image of a coronal section from a representative mouse showing the striatum imaging cannula window cortical lesion site. **j,**

Post-mortem image from a different mouse than **i** that was used for fiber photometry recording (fiber track indicated by arrow). **k,** Similarity of raw (no baseline normalization) whole-field GCaMP6f DF/F trace (top) with baseline normalized DF/F trace (bottom) for the example whole-field imaging session shown in Fig 1e. In the top trace, note the lack of baseline change over the recording session and particularly the stability of the baseline level during locomotion periods. Bottom trace is duplicate of trace in Fig. 1e.

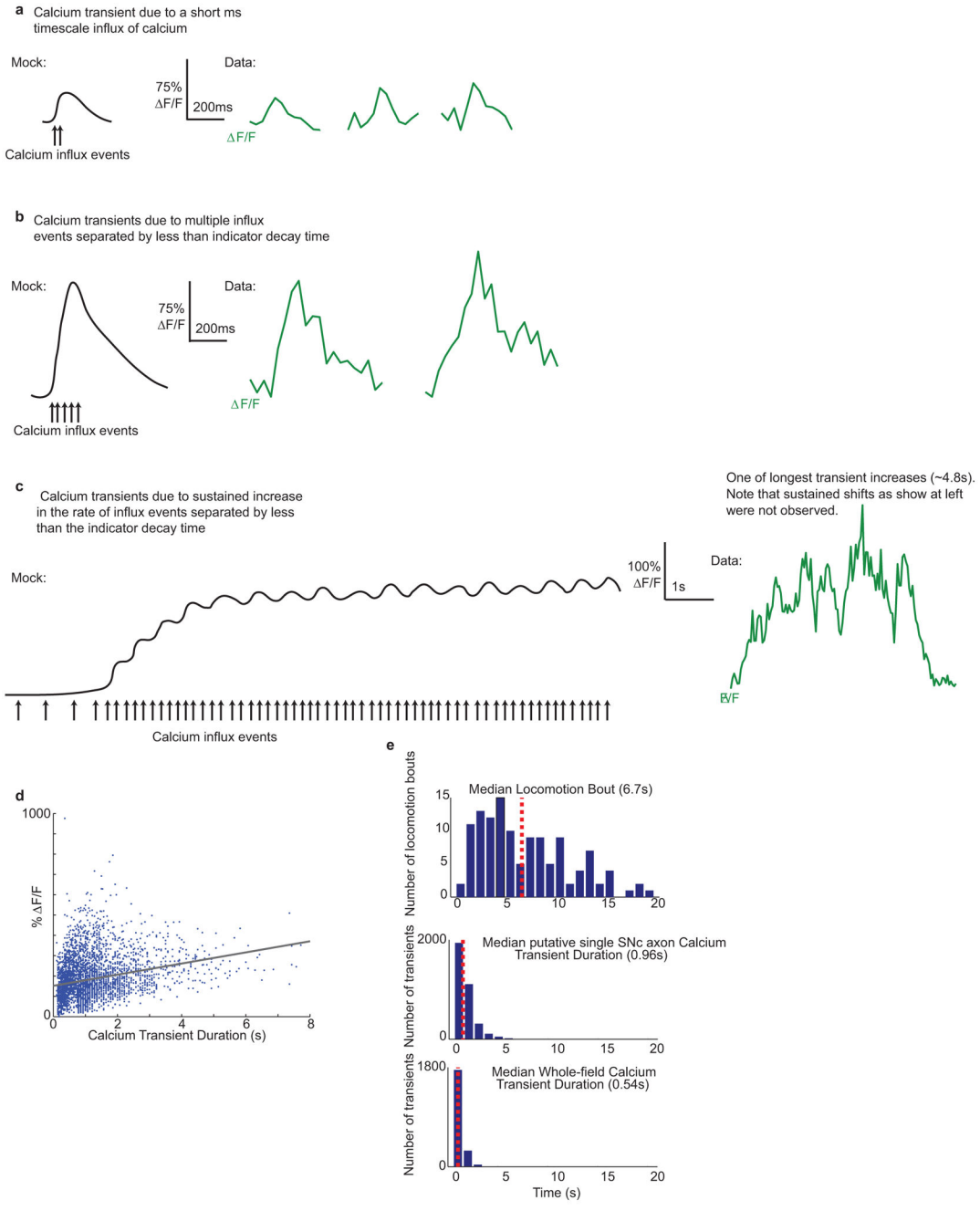

Extended Data Fig 3. Interpretation of mechanisms underlying calcium transients and characterization of putative single dopamine axon calcium transients

a, Left, Mock trace representing expected GCaMP6f calcium transient from a short millisecond timescale influx of calcium (arrows; e.g. short burst of action potentials over tens of milliseconds; local modulation may also contribute to calcium influx). Right, Three representative low-amplitude, short duration calcium transients (from putative single dopamine axons in dorsal striatum) (see Methods, Fig 4) that display onset and decay kinetics consistent with mock transient (left). **b,** Left, Mock trace representing expected GCaMP6f calcium transient from multiple calcium influx events separated by less than the indicator decay time (arrows; e.g. longer burst of action potential firing over ~100's of milliseconds). Right, representative larger amplitude calcium transients (from putative single dopamine axons in dorsal striatum) with rapid rise times consistent with mock transient (left). **c,** Left, Mock trace representing expected GCaMP6f calcium transient from a sustained increase in the rate of influx events separated by less than the decay time (e.g. sustained increase in action potential firing). Right, representative trace of one of the longest duration calcium transients observed (from putative single dopamine axons in dorsal striatum). Note that no sustained increases (baseline shifts) similar to the mock trace (left) were observed in single axon recordings or whole-field DF/F measurements; however, the long duration transient shown (right) indicates that if such sustained increases had occurred, they would have been detected using our methods. Also, note that the mock traces shown in **a–c** are for descriptive purposes and are not based on new data. These traces are based on two main assumptions: 1. DF/F is a monotonically increasing function of intracellular calcium concentration, which itself is a monotonically increasing function of the number of underlying action potentials (i.e. a greater number of action potentials leads to a larger DF/F, but the relationship is not necessarily linear), and 2. DF/F transients summate (not necessarily linearly) when they overlap in time. **d,** Duration vs. peak DF/F for all identified significant calcium transients in putative single SNc originating axons (see Methods, Fig 4, n = 3556 transients from 73 axons in 5 mice; Spearman's Rho = 0.3 $P<10^{-10}$). **e,** Histogram of sustained locomotion period durations (from SNc injected mice, n = 5, top) and calcium transient durations for all putative single SNc axons (n = 5 mice, mid) and all whole fields (n = 5 mice, bottom). Note that the median calcium transient duration (for either single axon or whole-field) is far less than the median locomotion duration, indicating that the increase in dopamine axon GCaMP6f DF/F observed during locomotion is due to an increase in relatively short duration calcium transients, rather than long-duration (sustained) increases in DF/F.

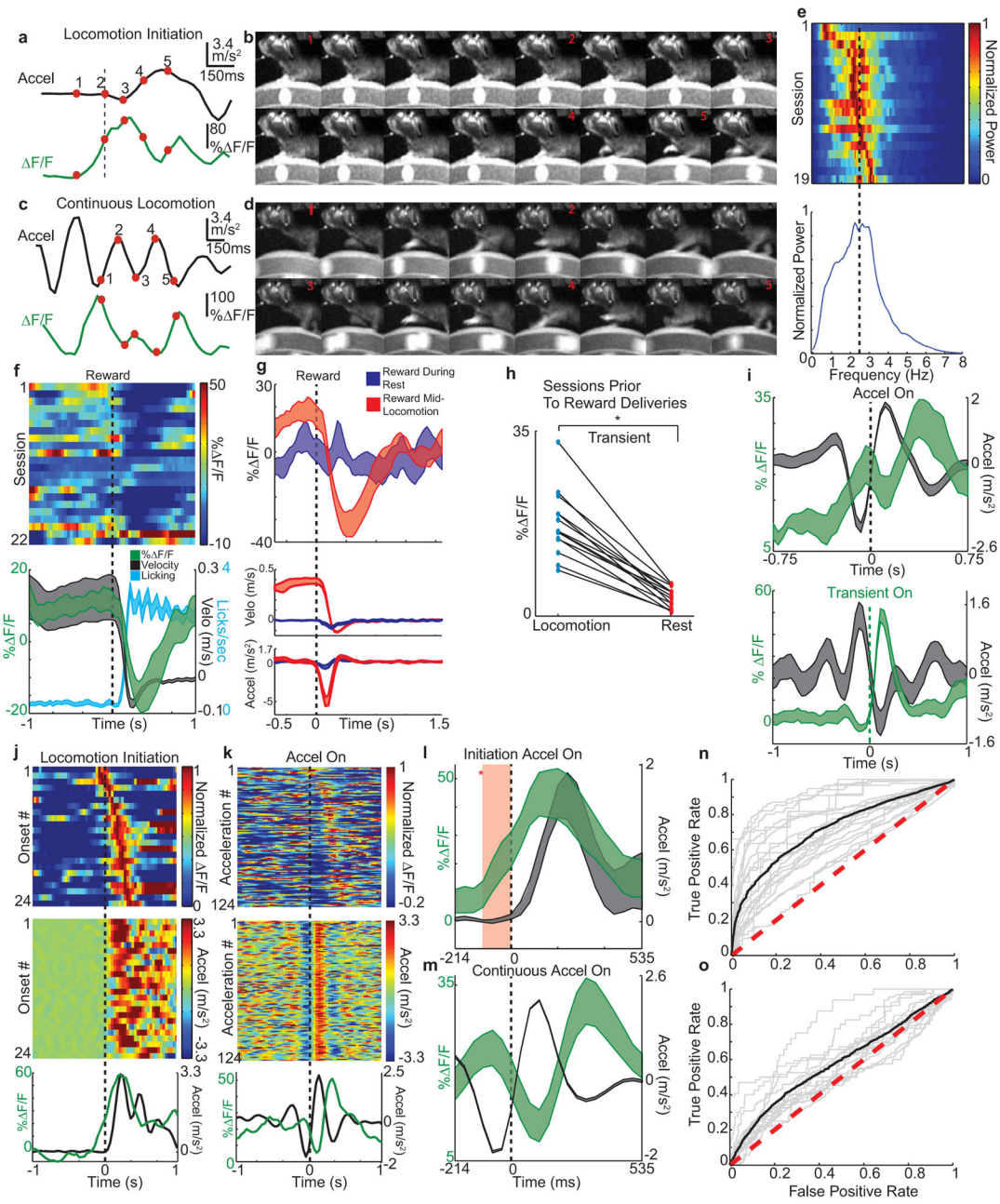

Extended Data Fig 4. Further characterization of acceleration-associated dopamine signaling

a, Representative whole-field D/DF fluorescence trace (one field from one out of 6 mice, green) aligned to treadmill acceleration (black) during a locomotion onset (dashed line: onset). **b,** Video frames of mouse for time points shown in **a. c, d** same as **a, b** but for a period of continuous locomotion. **e,** Top, Normalized spectral power of treadmill acceleration trace during continuous locomotion periods for each two-photon imaging session (each row represents a session, n = 6 mice). Bottom, Normalized mean power from all sessions shown in **e,** top. **f,** Top, Mean whole-field DF/F trace triggered on reward delivery time for all fields; each row is mean for each field/session (n = 22 fields, 6 mice).

Bottom, mean treadmill velocity (black), mean whole-field DF/F (green), and spout licking (light blue) all triggered on reward time (mean across all 22 fields/sessions in 6 mice). **g,** Mean whole-field DF/F (top), velocity (mid), and acceleration (bottom) for trials in which reward was delivered mid-locomotion (n = 13 sessions, 4 mice, red) or when animals were at rest (n = 12 sessions, 4 mice, blue). Note the sharp decrease in D/DF relative to baseline when animals decelerated from locomotion to consume the reward and the relative absence of phasic reward signaling when animals were given reward from rest. Reward responses were also not observed in single SNc axons when animals received reward from rest (see Extended Data Fig. 6). **h,** Comparison of mean whole-field fluorescence change from significant calcium transients (excluding baseline periods) between locomotion and resting periods; each point represents mean DF/F for running or resting over one session for each field (lines connect same field/session). All fields included here were imaged prior to mice ever receiving any rewards on the treadmill (n = 14 fields, 4 mice). *, $p < 10^{-5}$ (Wilcoxon Rank Sum Test). **i,** top, Mean acceleration (black) and whole-field DF/F (green) triggered on acceleration onsets (mean across all fields) during continuous locomotion. Bottom, Mean acceleration (black) triggered on all short duration calcium transients (green, mean of transients) during continuous locomotion across all fields. All fields included here were imaged prior to mice ever receiving any rewards on the treadmill (n = 14 fields, 4 mice). **j,** Top, Whole-field DF/F from all locomotion initiations in a representative single session (single imaging field, single session, one out of 6 mice); each row represents a single locomotion initiation time period (sorted by peak DF/F time). Mid, treadmill accelerations corresponding to locomotion initiations shown in **j**, top. Bottom, average of acceleration (black) and DF/F (green) across all locomotion onset traces displayed in Top and Mid panels. **k,** same as **j**, but for continuous locomotion periods. **l,** Reproduction of Figure 2e with zoomed-in time axes to show the timing of the mean DF/F in relation to the first acceleration at locomotion initiations from rest. Shaded red region indicates bins that were significantly (* $p < 0.01$ Wilcoxon, n = 15 fields in 6 mice) elevated relative to rest baseline. Shaded region covers ~107ms prior to acceleration onset. **m,** Reproduction of Figure 2f with zoomed-in time axes to show the timing of the mean dopamine transient in relation to the accelerations during continuous locomotion (n = 18 fields, 6 mice). **n**, ROC curves for each two-photon whole-field DF/F trace (n = 22 fields from 6 mice, grey; mean, black line) assessed for ability to discriminate locomotion versus resting periods (21/22 exhibited significant discriminability, $p < 0.01$). Mean area under the curve (AUC) = 0.76+/−0.02 S.E.M. **o**, ROC curves for each two-photon whole-field DF/F trace (n = 17 fields in 6 mice, grey; mean, black line) assessed for ability to discriminate pre-locomotion onset rest periods (250ms before onset) from other rest periods (10/17 exhibited significant discriminability, $p < 0.01$, 2 sessions included did not meet onset criteria for Fig 2e, Methods). Mean AUC = 0.58+/−0.02 S.E.M. Dashed red lines indicate the line of no discrimination. Shaded regions in **f, g, i, l, m** mean +/−s.e.m.

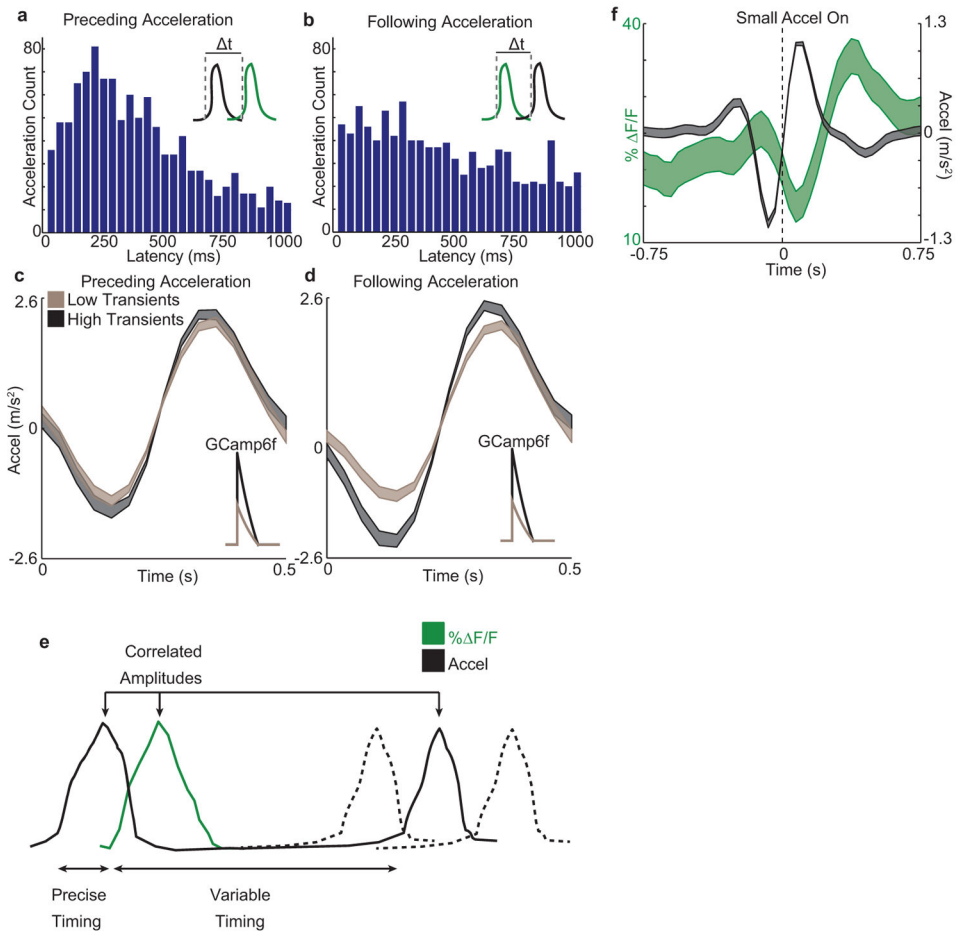

Extended Data Fig. 5. Dopamine axon calcium transients are temporally associated with preceding acceleration bursts and their amplitude is correlated with both preceding and subsequent acceleration bursts

a and b, Distribution of latencies from each significant calcium transient onset (mean whole-field fluorescence; 6 mice) to the first acceleration burst onset within 1s preceding (n = 1087, 6 mice **a**) or following (n = 990, 6 mice **b**) during continuous locomotion. Latencies are less variable (F-test for difference between variance of latencies, P = 7.1e-5) and shorter (Wilcoxon test for difference between latency means, P = 1.2e-5) to the preceding acceleration onsets, indicating more precise relative timing between the GCamp6f transients and the preceding acceleration burst versus the following acceleration burst. **c and d,** Mean acceleration traces from the first acceleration (within 1s) preceding (**c**) or following (**d**) all short duration (<0.5s) large amplitude (>75th percentile, n = 149 transients, grey) and small amplitude (<25th percentile, n = 149 transients, bronze) calcium transients occurring during continuous locomotion; aligned on acceleration onsets. Insets are schematics of the GCaMP6f transients. A significant correlation is present between the transient amplitudes and the immediately preceding acceleration amplitudes (Spearman's Rho = 0.16, P = 1.2e-4, from all transient-acceleration pairs; binned data from this plot shown in **c**). A significant correlation is also present between the transient amplitudes and the immediately following acceleration amplitudes (Spearman's Rho = 0.13, P = 0.006, from all transient-acceleration

pairs; binned data from this plot shown in **d**). **e**, Schematic summarizing relationship between the timing and amplitude of dopamine axon calcium transients and acceleration bursts during continuous locomotion. **f,** Mean acceleration (black) and whole-field DF/F (green) all triggered on all accelerations during continuous locomotion that were less than 1.7m/s^2 in amplitude (n = 596 accelerations, n = 6 mice); this demonstrates that dopamine axon GCaMP6f signaling displays a timing preference with respect to small amplitude accelerations, with similar timing and amplitude to that shown in Fig 2f (which includes both large and small amplitude accelerations).

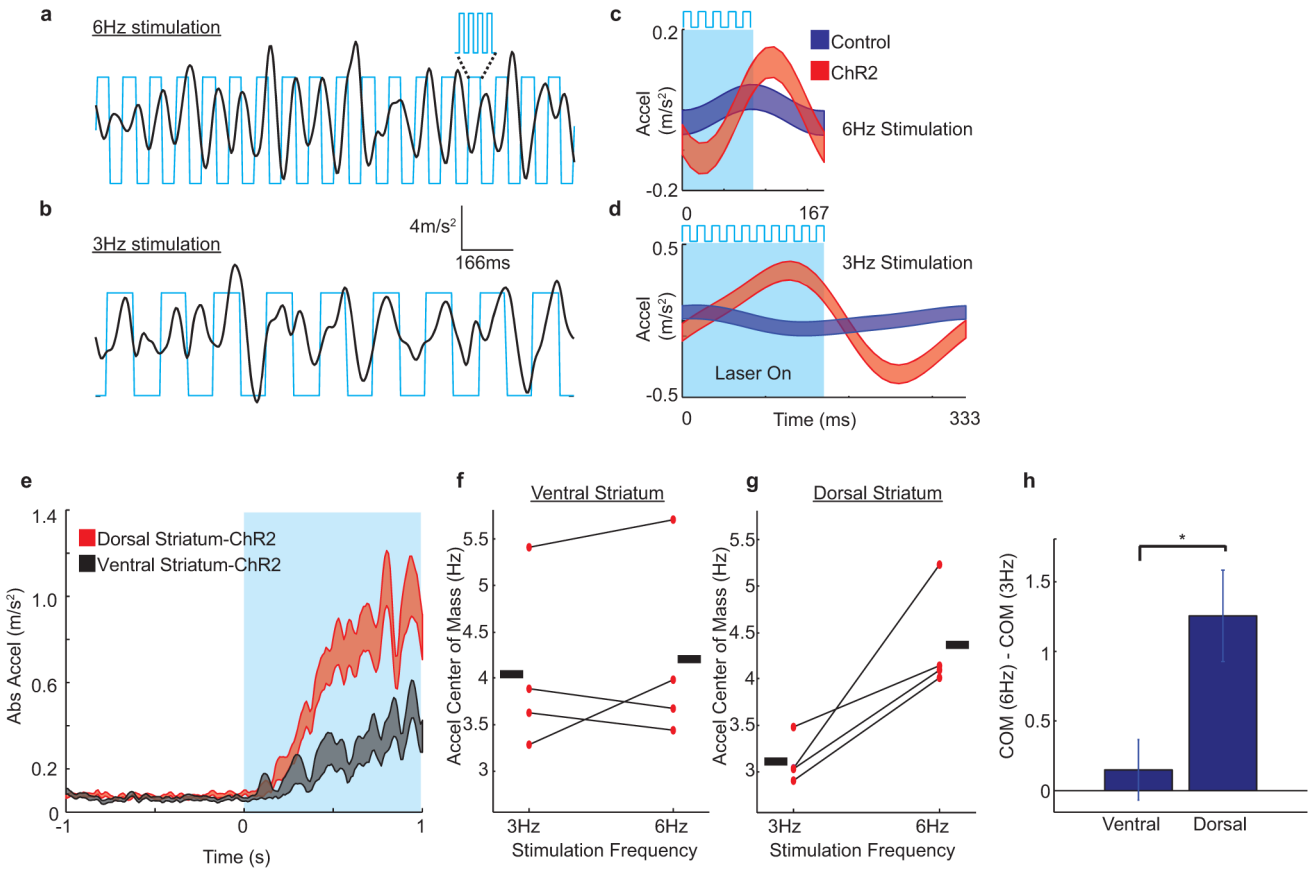

Extended Data Fig 6. Pulsed optogenetic stimulation of dorsal striatum projecting dopamine axons can entrain accelerations during locomotion (a–d); Pulsed optogenetic stimulation of ventral striatum projecting dopamine axons leads to little effect on locomotion (e–h)

a and b, Representative acceleration traces from continuous locomotion periods during (and initiated by) 6Hz (**a**) and 3Hz (**b**) laser stimulation trains in the same mouse. (Blue, laser stimulation train, one mouse out of 7). **c, d,** Mean accelerations triggered on individual laser burst onsets during continuous locomotion periods for 6Hz (**c**) and 3Hz (**d**) across all laser bursts in all mice and sessions (n = 7 mice). **e,** Mean absolute value of mouse accelerations aligned on onset of laser stimulation train applied to mice at rest (mean across all stimulation onsets, n = 55 and 91 for ventral and dorsal respectively, in all sessions and mice, 3 and 6Hz stimulation included). Dorsal and ventral striatum stimulations are from same ChR2 expressing mice (n=4). Three mice were not stimulated in ventral striatum and thus not

included in this figure. Mean acceleration elicited by ventral stimulation was significantly ($P < 0.01$, Wilcoxon Rank Sum Test) less than that elicited by dorsal axon stimulation. However, acceleration from ventral stimulation was significantly greater than chance ($P < 0.01$ shuffle test). This small effect in the ventral striatum could be due to activation of fibers which also project to dorsal striatum or to an increase in arousal. Though note that acceleration frequency during locomotion was not altered for stimulation in ventral striatum (see **f–d**). **f, g** Center of mass of acceleration power spectra for each mouse for locomotion periods initiated during 3 or 6Hz stimulations (n = 4 mice). Horizontal bars indicate means, lines connect same mouse. **h,** Mean difference between the center of mass of the acceleration power spectra computed for locomotion periods initiated during 3Hz or 6Hz axon stimulations in ventral (**f**) or dorsal (**g**) striatum. Positive values indicate a shift towards higher frequency accelerations for 6Hz stimulations (COM, center of mass of acceleration power spectrum). * $P < 0.05$ Wilcoxon Rank Sum Test.

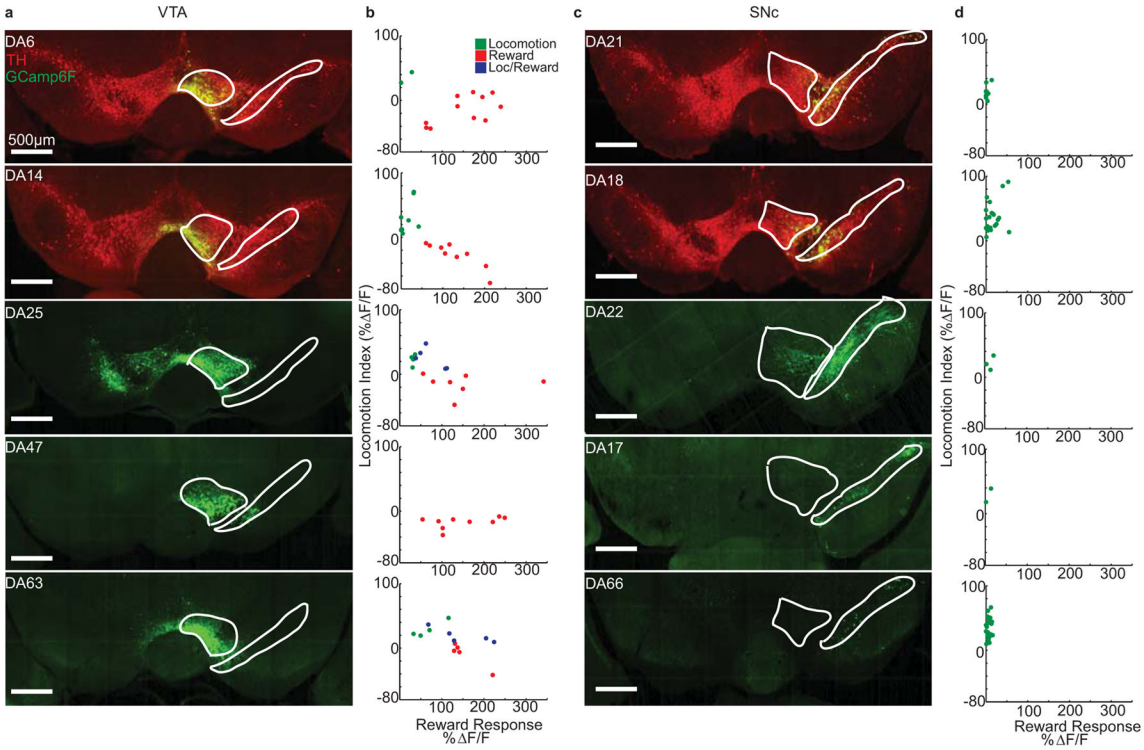

Extended Data Fig. 7. Histology and response distributions from each sparsely injected mouse

a, GCaMP6f expression (green) and TH immunofluorescence (red) from all VTA targeted mice (n = 5). **b,** Reward response vs locomotion index (as in Fig 4m) for each axon recorded from the corresponding mice in **a**. Green, significant locomotion; red, significant reward; blue both significant; neither significant not shown. **c and d,** Same as **a**, **b**, except from all SNc injected mice (n = 5). 6/10 mice were not stained for TH. Scalebars=500 µm.

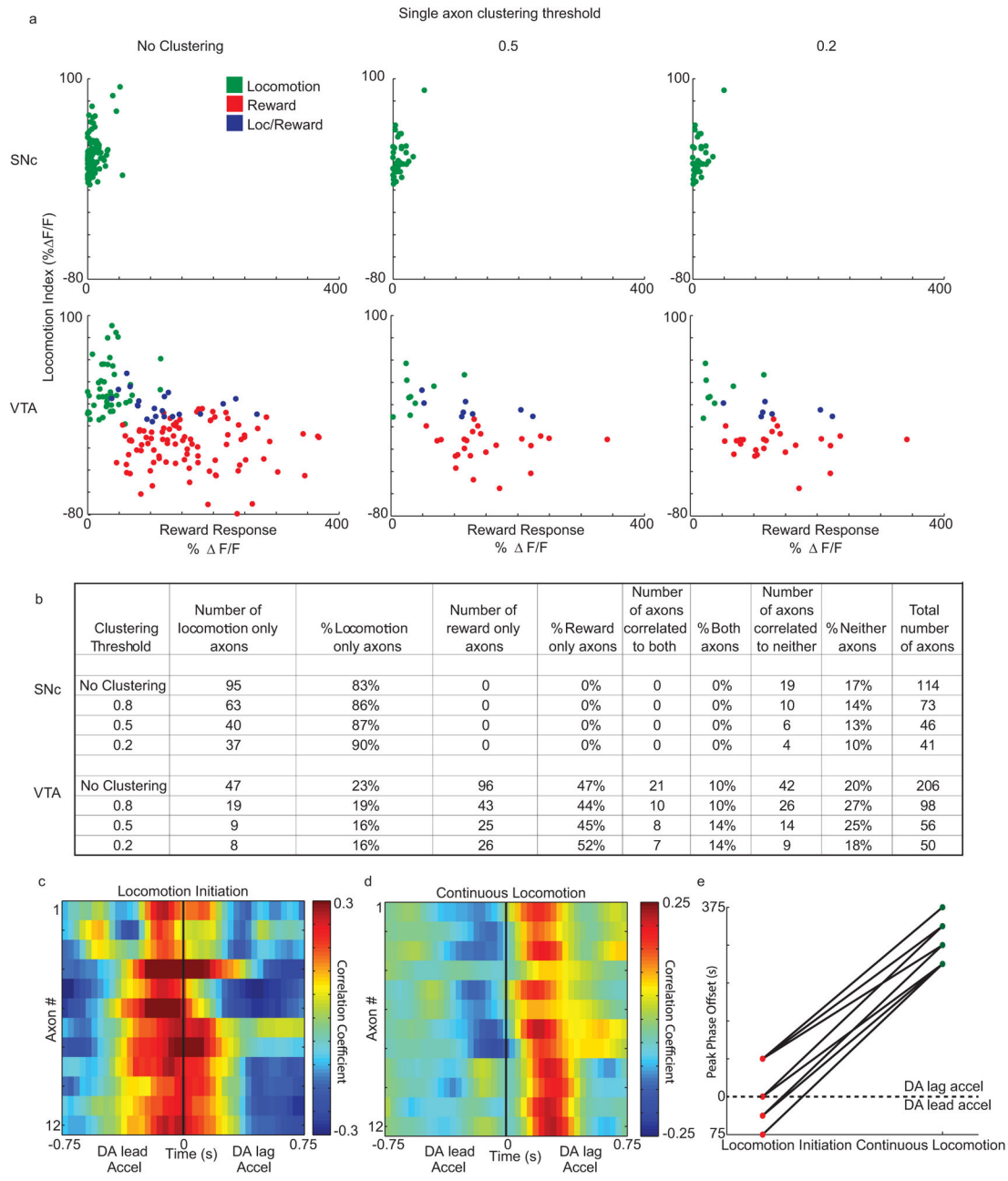

	Clustering Threshold	Number of locomotion only axons	% Locomotion only axons	Number of reward only axons	% Reward only axons	Number of axons correlated to both	% Both axons	Number of axons correlated to neither	% Neither axons	Total number of axons
SNc	No Clustering	95	83%	0	0%	0	0%	19	17%	114
	0.8	63	86%	0	0%	0	0%	10	14%	73
	0.5	40	87%	0	0%	0	0%	6	13%	46
	0.2	37	90%	0	0%	0	0%	4	10%	41
VTA	No Clustering	47	23%	96	47%	21	10%	42	20%	206
	0.8	19	19%	43	44%	10	10%	26	27%	98
	0.5	9	16%	25	45%	8	14%	14	25%	56
	0.2	8	16%	26	52%	7	14%	9	18%	50

Extended Data Fig 8. Distribution of reward and locomotion indexes and fraction of reward and locomotion signaling axons from VTA and SNc are highly similar using different correlation thresholds for clustering axon segments

a, Reward response vs. locomotion index for putative single axons from SNc (n = 5 mice, top row) and VTA (n = 5 mice, bottom row) using different correlation thresholds (No clustering, 0.5, and 0.2) for hierarchical clustering of activity patterns (see Methods). Axons are color-coded by significant responses to locomotion (green), reward (red), or both (blue). Note that despite the total number of putative axons decreasing with correlation threshold, the inverse relationship between locomotion and reward signaling across the population remains the same. **b,** Table showing the total numbers and fractions of responsive axons

across the VTA and SNc populations for different clustering thresholds. Note that despite the total number of putative axons decreasing with correlation threshold, the fraction of axons signaling either reward, locomotion, both or neither is highly similar. **c,** Correlations (Pearson's) between acceleration and selected putative single SNc axon DF/F traces at different relative time-lags (i.e. cross-correlations) during locomotion initiation periods; each row is mean for each axon for a single session (axons from n = 3/5 mice). **d,** Same as **c**, but during continuous locomotion periods; same axons during same sessions as in **c. e,** Peak cross-correlation times for data shown in **c, d** (lines connect same axons during same sessions).

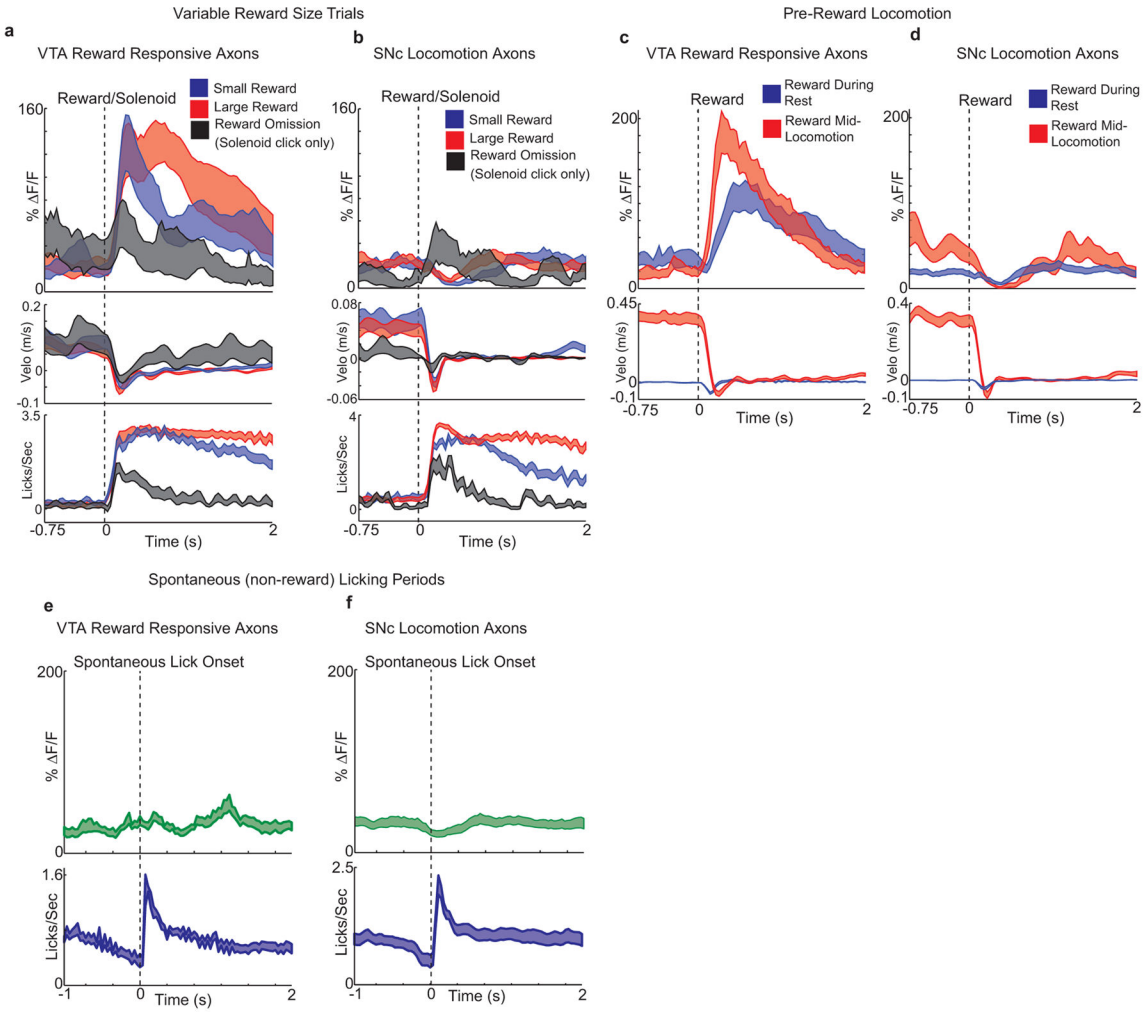

Extended Data Fig 9. Further characterization of putative single dopamine axons in relation to reward and licking

a, Mean DF/F trace for VTA reward responsive axons (Methods, n = 23 axons, n = 4 mice with variable reward sessions) (top), velocity (mid), and licking (bottom) triggered on large volume (red), small volume (blue) and omission (black, solenoid click was present, but no reward delivered; Methods, n = 17 axons, 3 mice with omission sessions) reward deliveries. **b,** Same as **a** except for SNc locomotion responsive axons (n = 62 and 18 axons for reward

and omission traces respectively). **c,** Mean VTA reward axon DF/F trace (top) and velocity (bottom) triggered on reward deliveries during continuous locomotion (red, n = 25 axons) or rest periods (blue, n = 37 axons). **d,** Same as **c** except for SNc locomotion responsive axons (n = 25 and 62 axons for locomotion and rest respectively). **e,** Mean VTA reward axon DF/F (top) and mouse licking (bottom) triggered on spontaneous, non-reward licking onsets (n = 15 axons, 3 mice). **f,** Same as **e** except for SNc locomotion responsive axons (n = 15 axons, 3 mice). Mice that did not outside reward periods were excluded. Shaded regions in **a–f**, mean +/− s.e.m.

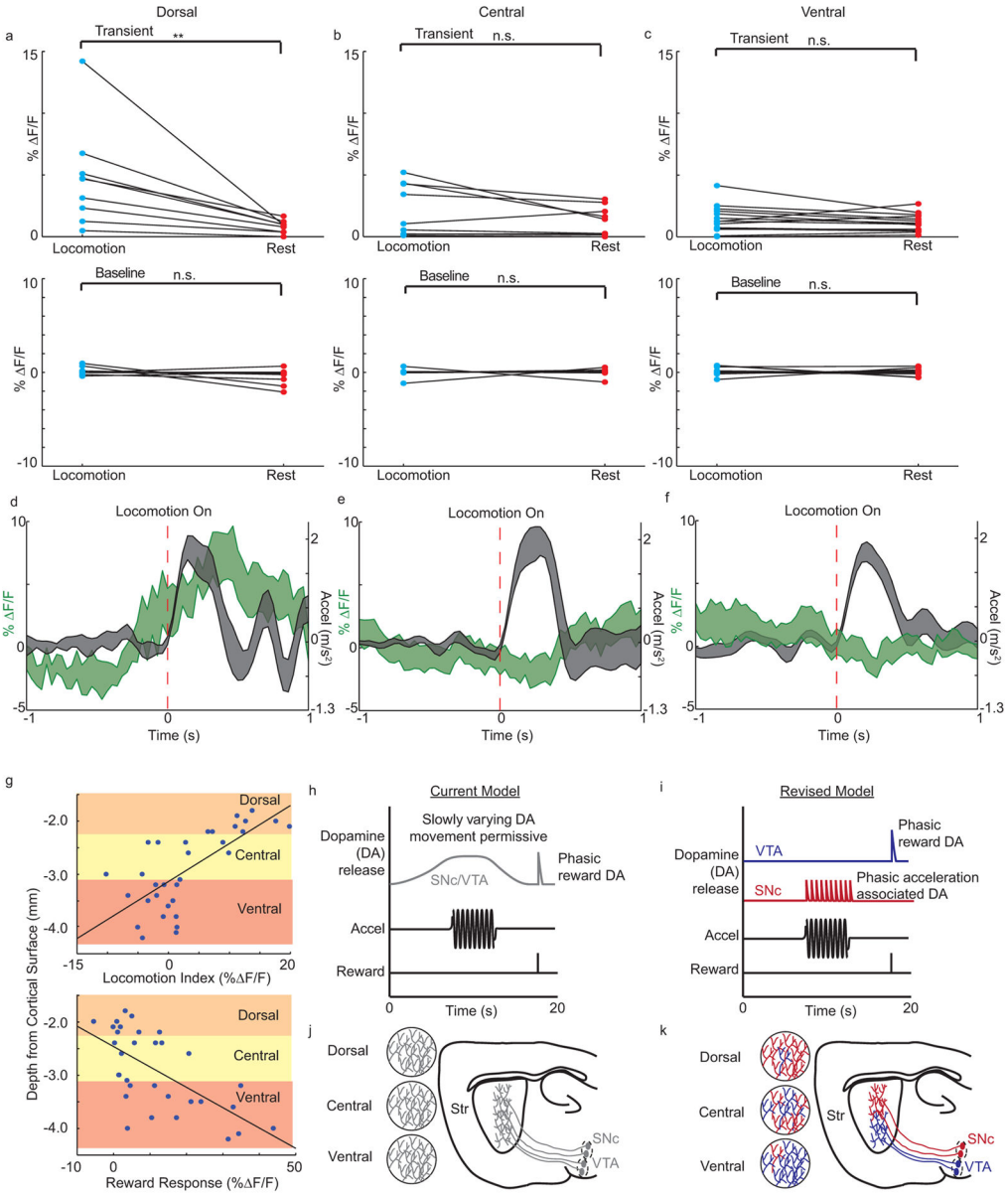

Extended Data Fig 10. Dopamine axon locomotion signaling measured by fiber photometry from different striatal sub regions

a, Top, Comparison of mean photometry fluorescence DF/F (mean of significant transients, excluding baseline periods) recorded from dorsal striatum between locomotion and resting periods; each point represents mean DF/F for running or resting over one session for recording from a single dorsal striatum location (lines connect same recording location/session; n = 5 mice). Bottom, Comparison of mean baseline (periods with no significant calcium transients) photometry DF/F recorded from dorsal striatum between locomotion and resting periods; each point represents mean baseline DF/F for running or resting over one session for recording from a single dorsal striatum location (lines connect same recording location/session, n = 5 mice). **b and c,** same as **a**, except for recordings from central and ventral striatum, respectively. **d,** Mean photometry DF/F recorded from dorsal striatum triggered on locomotion initiations (mean across all initiations, n = 5 mice). **e and f**, same as **d**, except for recordings from central and ventral striatum, respectively. **g,** Locomotion index (top) and reward response (bottom) vs. striatum recording depth (from data presented in Fig 5). **h,** Schematic of prominent current model for dopamine signaling dynamics in striatum. **i,** Schematic of our new model for dopamine signaling dynamics based on data presented here. **j and k,** Saggital schematics illustrating current homogenous dopamine signaling model (**j**) and our new model incorporating functional heterogeneity (**h**). **a–c**, **, $p < 0.01$ (Wilcoxon Rank Sum Test); n.s., not significant. Shaded regions in **d–f**, mean +/− s.e.m across initiations (n = 20, 28, and 56 from dorsal, central, and ventral respectively in 5 mice).

Supplementary Material

Refer to Web version on PubMed Central for supplementary material.

Acknowledgments

We thank A. Graybiel and members of the Dombeck lab for comments on the manuscript, V. Jayaraman, R. Kerr, D. Kim, L. Looger, K. Svoboda from the GENIE Project (Janelia Farm, Howard Hughes Medical Institute) for GCaMP6. This work was supported by Klingenstein Foundation, McKnight Foundation, Whitehall Foundation, Chicago Biomedical Consortium with support from the Searle Funds at Chicago Community Trust, Northwestern University, National Institutes of Health (T32 AG20506).

References

1. Dauer W, Przedborski S. Parkinson’s disease: mechanisms and models. Neuron. 2003; 39:889–909. [PubMed: 12971891]
2. Hornykiewicz O. Dopamine (3-hydroxytyramine) in the central nervous system and its relation to the Parkinson syndrome in man. Deutsche medizinische Wochenschrift. 1962; 87:1807–1810. DOI: 10.1055/s-0028-1114024 [PubMed: 14448985]
3. Carlsson A. Evidence for a Role of Dopamine in Extrapyramidal Functions. Acta neurovegetativa. 1964; 26:484–493. [PubMed: 14317354]
4. Day JJ, Roitman MF, Wightman RM, Carelli RM. Associative learning mediates dynamic shifts in dopamine signaling in the nucleus accumbens. Nature neuroscience. 2007; 10:1020–1028. DOI: 10.1038/nn1923 [PubMed: 17603481]
5. Howe MW, Tierney PL, Sandberg SG, Phillips PE, Graybiel AM. Prolonged dopamine signalling in striatum signals proximity and value of distant rewards. Nature. 2013; 500:575–579. DOI: 10.1038/nature12475 [PubMed: 23913271]
6. Romo R, Schultz W. Dopamine neurons of the monkey midbrain: contingencies of responses to active touch during self-initiated arm movements. Journal of neurophysiology. 1990; 63:592–606. [PubMed: 2329363]

7. Pan WX, Schmidt R, Wickens JR, Hyland BI. Dopamine cells respond to predicted events during classical conditioning: evidence for eligibility traces in the reward-learning network. The Journal of neuroscience : the official journal of the Society for Neuroscience. 2005; 25:6235–6242. DOI: 10.1523/JNEUROSCI.1478-05.2005 [PubMed: 15987953]
8. Cohen JY, Haesler S, Vong L, Lowell BB, Uchida N. Neuron-type-specific signals for reward and punishment in the ventral tegmental area. Nature. 2012; 482:85–88. DOI: 10.1038/nature10754 [PubMed: 22258508]
9. Mirenowicz J, Schultz W. Importance of unpredictability for reward responses in primate dopamine neurons. Journal of neurophysiology. 1994; 72:1024–1027. [PubMed: 7983508]
10. Hamid AA, et al. Mesolimbic dopamine signals the value of work. Nature neuroscience. 2016; 19:117–126. DOI: 10.1038/nn.4173 [PubMed: 26595651]
11. Berridge KC. The debate over dopamine's role in reward: the case for incentive salience. Psychopharmacology. 2007; 191:391–431. DOI: 10.1007/s00213-006-0578-x [PubMed: 17072591]
12. Schultz W. Multiple dopamine functions at different time courses. Annual review of neuroscience. 2007; 30:259–288. DOI: 10.1146/annurev.neuro.28.061604.135722
13. Schultz W, Dayan P, Montague PR. A neural substrate of prediction and reward. Science. 1997; 275:1593–1599. [PubMed: 9054347]
14. Mazzoni P, Hristova A, Krakauer JW. Why don't we move faster? Parkinson's disease, movement vigor, and implicit motivation. The Journal of neuroscience : the official journal of the Society for Neuroscience. 2007; 27:7105–7116. DOI: 10.1523/JNEUROSCI.0264-07.2007 [PubMed: 17611263]
15. Niv Y, Daw ND, Joel D, Dayan P. Tonic dopamine: opportunity costs and the control of response vigor. Psychopharmacology. 2007; 191:507–520. DOI: 10.1007/s00213-006-0502-4 [PubMed: 17031711]
16. Jin X, Costa RM. Start/stop signals emerge in nigrostriatal circuits during sequence learning. Nature. 2010; 466:457–462. DOI: 10.1038/nature09263 [PubMed: 20651684]
17. Puryear CB, Kim MJ, Mizumori SJ. Conjunctive encoding of movement and reward by ventral tegmental area neurons in the freely navigating rodent. Behavioral neuroscience. 2010; 124:234–247. DOI: 10.1037/a0018865 [PubMed: 20364883]
18. Tobler PN, Fiorillo CD, Schultz W. Adaptive coding of reward value by dopamine neurons. Science. 2005; 307:1642–1645. DOI: 10.1126/science.1105370 [PubMed: 15761155]
19. Roesch MR, Calu DJ, Schoenbaum G. Dopamine neurons encode the better option in rats deciding between differently delayed or sized rewards. Nature neuroscience. 2007; 10:1615–1624. DOI: 10.1038/nn2013 [PubMed: 18026098]
20. Barter JW, et al. Beyond reward prediction errors: the role of dopamine in movement kinematics. Frontiers in integrative neuroscience. 2015; 9:39. [PubMed: 26074791]
21. Dodson PD, et al. Representation of spontaneous movement by dopaminergic neurons is cell-type selective and disrupted in parkinsonism. Proceedings of the National Academy of Sciences of the United States of America. 2016
22. Margolis EB, Lock H, Hjelmstad GO, Fields HL. The ventral tegmental area revisited: is there an electrophysiological marker for dopaminergic neurons? The Journal of physiology. 2006; 577:907–924. DOI: 10.1113/jphysiol.2006.117069 [PubMed: 16959856]
23. Wang L, et al. Modulation of dopamine release in the striatum by physiologically relevant levels of nicotine. Nature communications. 2014; 5:3925.
24. Threlfell S, et al. Striatal dopamine release is triggered by synchronized activity in cholinergic interneurons. Neuron. 2012; 75:58–64. DOI: 10.1016/j.neuron.2012.04.038 [PubMed: 22794260]
25. Robinson DL, Venton BJ, Heien ML, Wightman RM. Detecting subsecond dopamine release with fast-scan cyclic voltammetry in vivo. Clinical chemistry. 2003; 49:1763–1773. [PubMed: 14500617]
26. Dombeck DA, Harvey CD, Tian L, Looger LL, Tank DW. Functional imaging of hippocampal place cells at cellular resolution during virtual navigation. Nature neuroscience. 2010; 13:1433–1440. DOI: 10.1038/nn.2648 [PubMed: 20890294]

27. Chen TW, et al. Ultrasensitive fluorescent proteins for imaging neuronal activity. Nature. 2013; 499:295–300. DOI: 10.1038/nature12354 [PubMed: 23868258]
28. Matsuda W, et al. Single nigrostriatal dopaminergic neurons form widely spread and highly dense axonal arborizations in the neostriatum. The Journal of neuroscience : the official journal of the Society for Neuroscience. 2009; 29:444–453. DOI: 10.1523/JNEUROSCI.4029-08.2009 [PubMed: 19144844]
29. Petreanu L, et al. Activity in motor-sensory projections reveals distributed coding in somatosensation. Nature. 2012; 489:299–303. DOI: 10.1038/nature11321 [PubMed: 22922646]
30. Cox CL, Denk W, Tank DW, Svoboda K. Action potentials reliably invade axonal arbors of rat neocortical neurons. Proceedings of the National Academy of Sciences of the United States of America. 2000; 97:9724–9728. DOI: 10.1073/pnas.170278697 [PubMed: 10931955]
31. Turner TJ. Nicotine enhancement of dopamine release by a calcium-dependent increase in the size of the readily releasable pool of synaptic vesicles. The Journal of neuroscience : the official journal of the Society for Neuroscience. 2004; 24:11328–11336. DOI: 10.1523/JNEUROSCI.1559-04.2004 [PubMed: 15601939]
32. Woodward JJ, Chandler LJ, Leslie SW. Calcium-dependent and -independent release of endogenous dopamine from rat striatal synaptosomes. Brain research. 1988; 473:91–98. [PubMed: 3208129]
33. Tritsch NX, Ding JB, Sabatini BL. Dopaminergic neurons inhibit striatal output through non-canonical release of GABA. Nature. 2012; 490:262–266. DOI: 10.1038/nature11466 [PubMed: 23034651]
34. Parker NF, et al. Reward and choice encoding in terminals of midbrain dopamine neurons depends on striatal target. Nature neuroscience. 2016
35. Boyden ES, Zhang F, Bamberg E, Nagel G, Deisseroth K. Millisecond-timescale, genetically targeted optical control of neural activity. Nature neuroscience. 2005; 8:1263–1268. DOI: 10.1038/nn1525 [PubMed: 16116447]
36. Ikemoto S. Dopamine reward circuitry: two projection systems from the ventral midbrain to the nucleus accumbens-olfactory tubercle complex. Brain research reviews. 2007; 56:27–78. DOI: 10.1016/j.brainresrev.2007.05.004 [PubMed: 17574681]
37. Hollerman JR, Schultz W. Dopamine neurons report an error in the temporal prediction of reward during learning. Nature neuroscience. 1998; 1:304–309. DOI: 10.1038/1124 [PubMed: 10195164]
38. Schultz W, Romo R. Dopamine neurons of the monkey midbrain: contingencies of responses to stimuli eliciting immediate behavioral reactions. Journal of neurophysiology. 1990; 63:607–624. [PubMed: 2329364]
39. Lerner TN, et al. Intact-Brain Analyses Reveal Distinct Information Carried by SNc Dopamine Subcircuits. Cell. 2015; 162:635–647. DOI: 10.1016/j.cell.2015.07.014 [PubMed: 26232229]
40. Salamone JD, Correa M. The mysterious motivational functions of mesolimbic dopamine. Neuron. 2012; 76:470–485. DOI: 10.1016/j.neuron.2012.10.021 [PubMed: 23141060]
41. Dombeck DA, Khabbaz AN, Collman F, Adelman TL, Tank DW. Imaging large-scale neural activity with cellular resolution in awake, mobile mice. Neuron. 2007; 56:43–57. DOI: 10.1016/j.neuron.2007.08.003 [PubMed: 17920014]
42. Steinberg EE, Janak PH. Establishing causality for dopamine in neural function and behavior with optogenetics. Brain research. 2013; 1511:46–64. DOI: 10.1016/j.brainres.2012.09.036 [PubMed: 23031636]
43. Steinbeck JA, et al. Optogenetics enables functional analysis of human embryonic stem cell-derived grafts in a Parkinson's disease model. Nature biotechnology. 2015; 33:204–209. DOI: 10.1038/nbt.3124
44. Lammel S, et al. Input-specific control of reward and aversion in the ventral tegmental area. Nature. 2012; 491:212–217. DOI: 10.1038/nature11527 [PubMed: 23064228]
45. Beier KT, et al. Circuit Architecture of VTA Dopamine Neurons Revealed by Systematic Input-Output Mapping. Cell. 2015; 162:622–634. DOI: 10.1016/j.cell.2015.07.015 [PubMed: 26232228]
46. Poulin JF, et al. Defining midbrain dopaminergic neuron diversity by single-cell gene expression profiling. Cell reports. 2014; 9:930–943. DOI: 10.1016/j.celrep.2014.10.008 [PubMed: 25437550]

47. Roeper J. Dissecting the diversity of midbrain dopamine neurons. Trends in neurosciences. 2013; 36:336–342. DOI: 10.1016/j.tins.2013.03.003 [PubMed: 23582338]

48. Lammel S, et al. Diversity of transgenic mouse models for selective targeting of midbrain dopamine neurons. Neuron. 2015; 85:429–438. DOI: 10.1016/j.neuron.2014.12.036 [PubMed: 25611513]

49. Matsumoto M, Hikosaka O. Two types of dopamine neuron distinctly convey positive and negative motivational signals. Nature. 2009; 459:837–841. DOI: 10.1038/nature08028 [PubMed: 19448610]

50. Gunaydin LA, et al. Natural neural projection dynamics underlying social behavior. Cell. 2014; 157:1535–1551. DOI: 10.1016/j.cell.2014.05.017 [PubMed: 24949967]

51. Dombeck DA, Harvey CD, Tian L, Looger LL, Tank DW. Functional imaging of hippocampal place cells at cellular resolution during virtual navigation. Nature neuroscience. 2010; 13:1433–1440. DOI: 10.1038/nn.2648 [PubMed: 20890294]

52. Harvey CD, Collman F, Dombeck DA, Tank DW. Intracellular dynamics of hippocampal place cells during virtual navigation. Nature. 2009; 461:941–946. DOI: 10.1038/nature08499 [PubMed: 19829374]

53. Heys JG, Rangarajan KV, Dombeck DA. The functional micro-organization of grid cells revealed by cellular-resolution imaging. Neuron. 2014; 84:1079–1090. DOI: 10.1016/j.neuron.2014.10.048 [PubMed: 25467986]

54. Sheffield ME, Dombeck DA. Calcium transient prevalence across the dendritic arbour predicts place field properties. Nature. 2015; 517:200–204. DOI: 10.1038/nature13871 [PubMed: 25363782]

55. Chen TW, et al. Ultrasensitive fluorescent proteins for imaging neuronal activity. Nature. 2013; 499:295–300. DOI: 10.1038/nature12354 [PubMed: 23868258]

56. Cox CL, Denk W, Tank DW, Svoboda K. Action potentials reliably invade axonal arbors of rat neocortical neurons. Proceedings of the National Academy of Sciences of the United States of America. 2000; 97:9724–9728. DOI: 10.1073/pnas.170278697 [PubMed: 10931955]

57. Hofer SB, et al. Differential connectivity and response dynamics of excitatory and inhibitory neurons in visual cortex. Nature neuroscience. 2011; 14:1045–1052. DOI: 10.1038/nn.2876 [PubMed: 21765421]

58. Miyashita T, Shao YR, Chung J, Pourzia O, Feldman DE. Long-term channelrhodopsin-2 (ChR2) expression can induce abnormal axonal morphology and targeting in cerebral cortex. Front Neural Circuits. 2013; 7:8. [PubMed: 23386813]

59. Miri A, et al. Spatial gradients and multidimensional dynamics in a neural integrator circuit. Nature neuroscience. 2011; 14:1150–1159. DOI: 10.1038/nn.2888 [PubMed: 21857656]

60. Mukamel EA, Nimmerjahn A, Schnitzer MJ. Automated analysis of cellular signals from large-scale calcium imaging data. Neuron. 2009; 63:747–760. DOI: 10.1016/j.neuron.2009.08.009 [PubMed: 19778505]

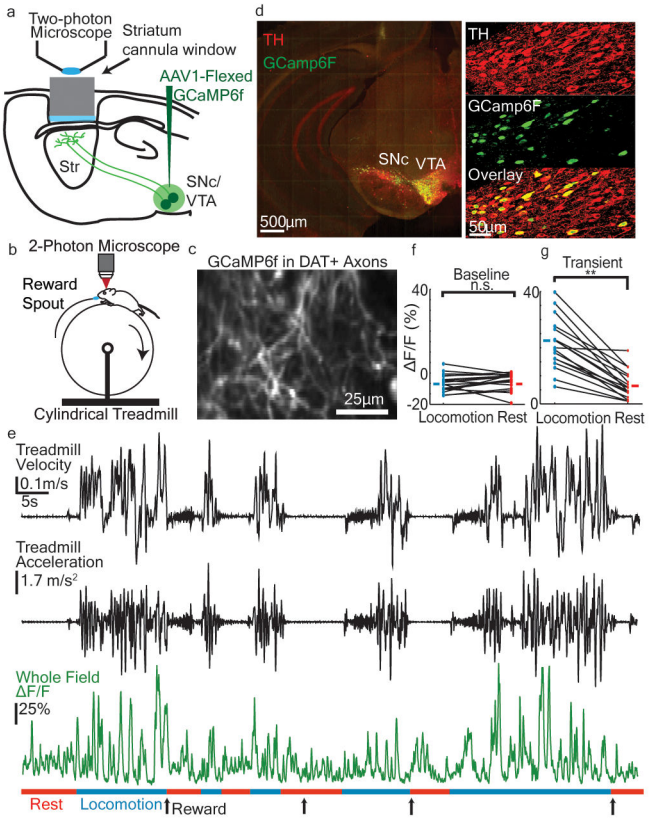

Fig 1. Locomotion related signaling in dorsal striatal projecting dopamine axons

a, Schematic of methods. **b,** Mouse running on treadmill under microscope. **c,** Representative field of GCaMP6f labeled dopamine axons in dorsal striatum. **d,** GCamp6f expression in dopamine neurons (green) overlaid with TH immunofluorescence (red). Right insets are high-zoom. **e,** Average whole field DF/F fluorescence from a representative field in one mouse (bottom, n = 6 mice total) and corresponding treadmill velocity (top) and acceleration (middle) during locomotion. **f,** Comparison of mean baseline (periods with no significant calcium transients) whole-field DF/F between locomotion and resting periods. **g**, Comparison of mean whole-field fluorescence change (mean of significant calcium transients, excluded baseline periods) between locomotion and resting periods. **f**, **g**, each point represents mean baseline DF/F for running or resting over one session for each field (n = 17 sessions from 6 mice, lines connect same field/session, short lines: mean over sessions); **, $p < 10^{-5}$, Wilcoxon Rank Sum Test.

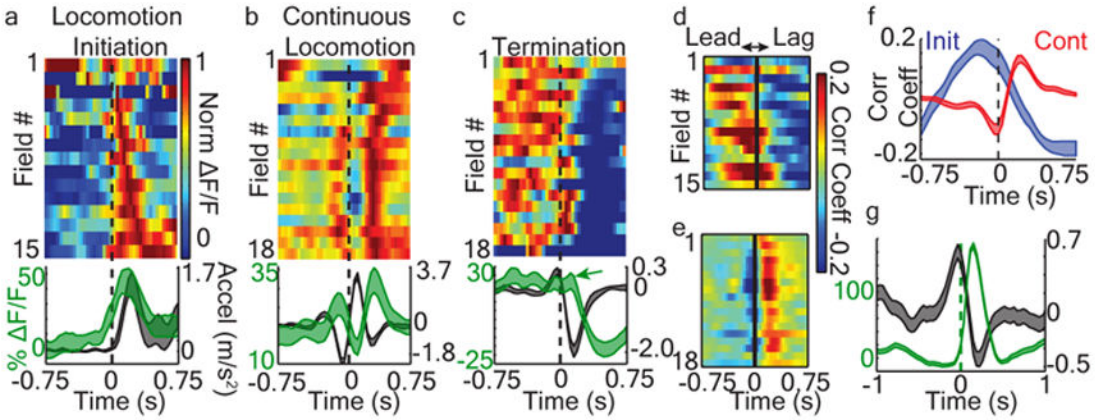

Fig 2. Phasic dopamine signaling displays a sub-second timing preference with respect to acceleration bursts

a, Top, Mean of whole-field DF/F triggered on accelerations at locomotion initiations; each row is mean for each field/session (DF/F normalized for each row and sorted by peak time). Bottom, Mean acceleration (black) and whole-field DF/F (green) all triggered on locomotion initiations (mean across all fields). **b**, Same as **a**, except triggered on accelerations during continuous locomotion periods. **c,** Same as **a**, except triggered on locomotion terminations; note lack of DF/F transient peak (arrow) following final acceleration. **d,** Correlations between acceleration and whole-field fluorescence at different relative time-lags (i.e. cross-correlations) during locomotion initiation periods (sorted by peak correlation time); each row is mean for each field/session. **e,** Same as **d**, but during continuous locomotion periods. **f,** Mean cross-correlations between acceleration and whole-field fluorescence for initiation (blue) and continuous (red) locomotion periods. **g,** Mean acceleration (black) triggered on all short duration calcium transients (green, mean of transients) during continuous locomotion across all fields. Shaded regions in **a, b, c, f, g** mean +/− s.e.m. **a–f** include all n=6 mice.

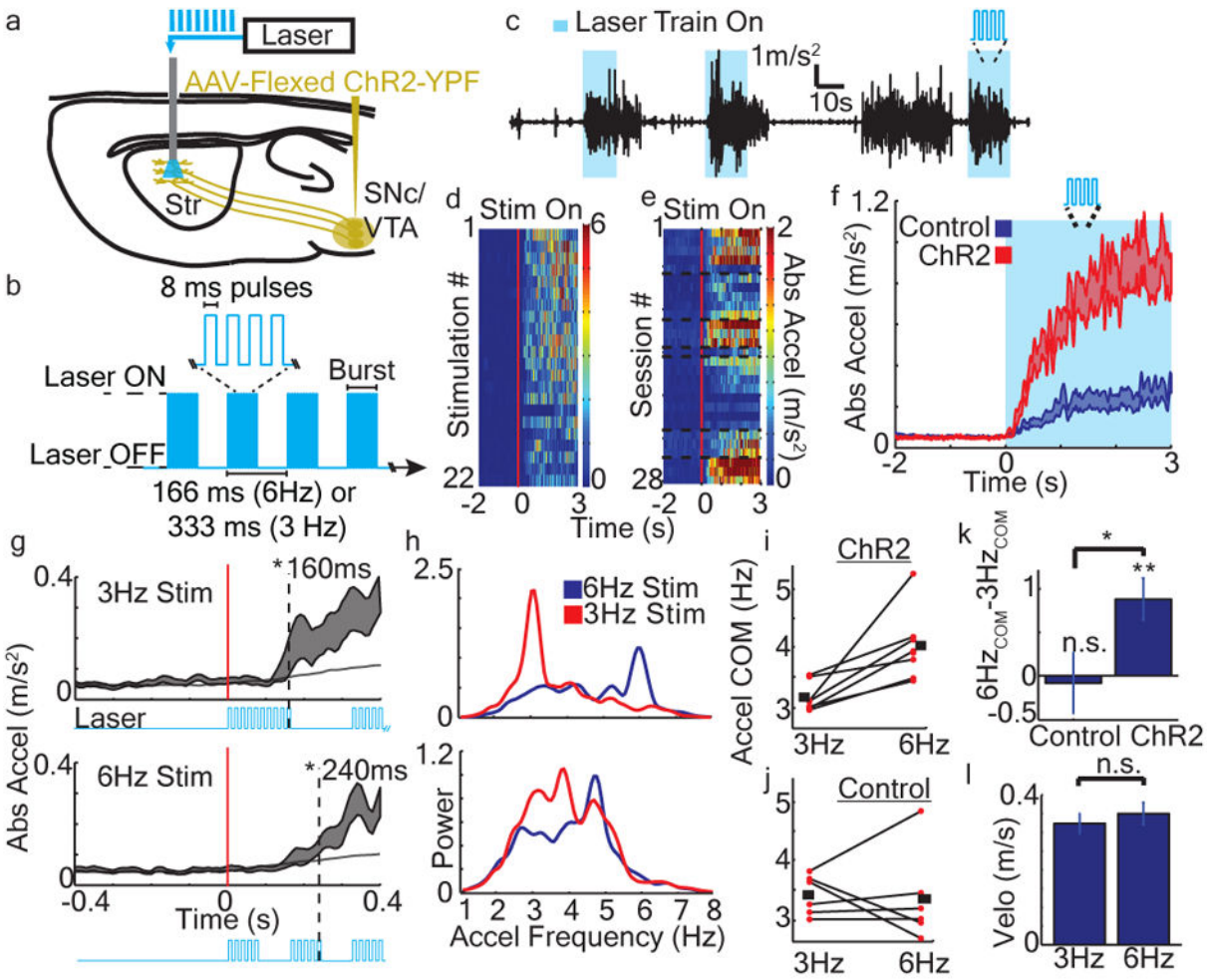

Fig 3. Pulsed optogenetic stimulation of dorsal striatum projecting dopamine axons can rapidly initiate locomotion and control acceleration frequency

a, Schematic of methods. **b,** Pulsed laser delivery protocol for dopamine axon ChR2 stimulation (used for all data presented in this paper). **c,** Representative acceleration from a single stimulation session (blue regions, laser train stimulation to dorsal striatum). **d,** Absolute value of mouse acceleration aligned on onset of all laser stimulation trains (red line) during a representative single session from one mouse (n = 7 mice total, each row represents a single trial stimulation from rest). **e,** All mean accelerations aligned on laser stimulation trains applied to mice at rest (each row represents mean over one session; rows corresponding to sessions for each mouse grouped together; sessions from different mice separated by dashed lines). **f,** Mean absolute value of mouse accelerations aligned on the onsets of laser stimulation trains applied to mice at rest (mean across all stimulation onsets, n = 161 and 267 onsets for ChR2 and control respectively, in all sessions and mice, 3 and 6Hz stimulation included). **g,** Same data as **f**, but stimulations separated into 3 or 6 Hz groups and zoomed-in time (blue, laser stimulation). Dashed lines, time when acceleration becomes significantly ($P<0.01$) greater than random shuffle (thin grey line, mean random shuffle). **h,** Power spectra of acceleration for two representative mice during locomotion periods initiated during 3 and 6Hz stimulations. **i and j,** Center of mass of acceleration

power spectra for each ChR2 (**i**) or control (**j**) mouse for locomotion periods initiated during 3 and 6Hz stimulations. Horizontal bars indicate means, lines connect same mouse. **k,** Mean difference between center of mass of acceleration power spectra during 3Hz and 6Hz stimulations (differences calculated for each mouse) averaged across control or ChR2 mice (COM, center of mass of acceleration power spectrum). **l,** Mean velocity across mice during 6Hz and 3Hz stimulations included in **k**. Shaded regions in **f,g** mean +/− s.e.m. **k,**** $P < 0.01$ (compared to 0),* $P < 0.05$; **l,** n.s. $P>0.05$ Wilcoxon Rank Sum test.

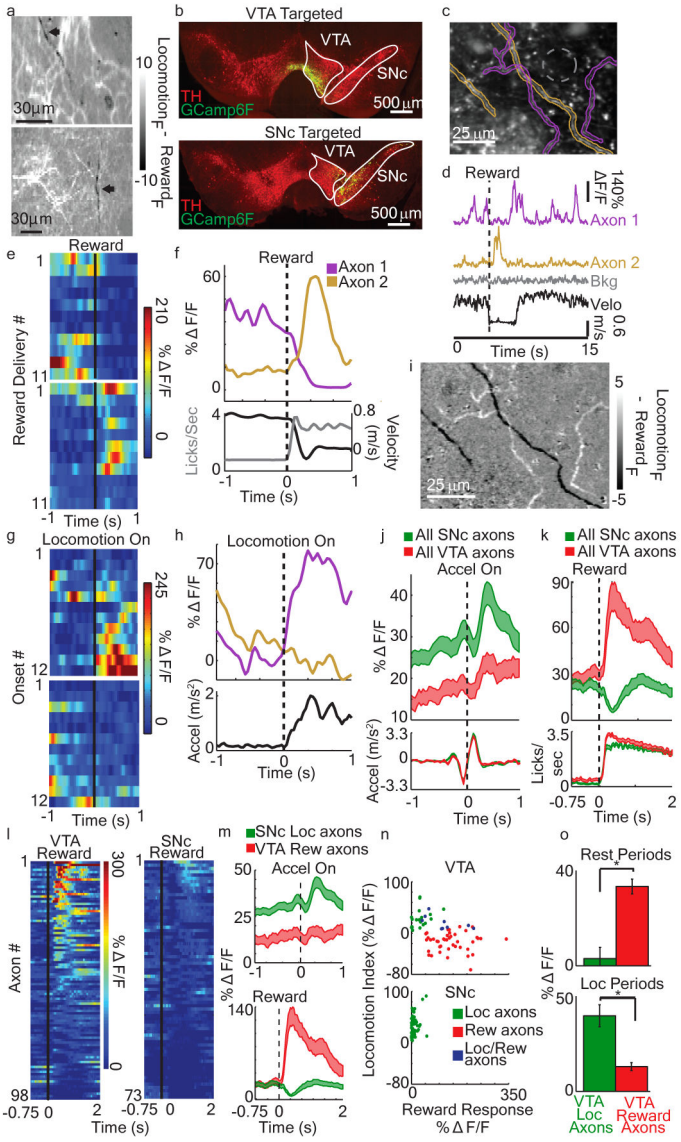

Fig 4. Functional heterogeneity and anatomical origin of dorsal striatum projecting dopamine axons

a, Mean image during locomotion periods minus mean image during reward periods for two representative dopamine axon fields (arrows, axon segments signaling more during reward). **b,** Coronal sections showing restricted GCamp6f expression (green) in VTA (top) and SNc (bottom) overlaid with TH immunofluorescence (red). **c,** Representative maximum fluorescence projection image from one field in a mouse with GCaMP6f expression localized to VTA (n = 5 total VTA targeted mice). Gold and purple regions are identified ROIs from putative single axons (grey, background). **d,** DF/F from ROIs in **c** aligned with treadmill velocity and reward time. **e,** Reward triggered DF/F from the purple (top) and gold (bottom) ROIs from **c**; each row represents a single reward delivery. **f,** Mean reward-triggered DF/F (gold, purple, top), velocity (black, bottom) and licking (grey, bottom) for the two axons in **c** over the recording session. **g, h,** Same as **e**, **f**, except triggered on locomotion

onsets. **i,** same as **a**, but for field shown in **c. j,** Mean DF/F triggered on acceleration onsets for all putative single axons from all SNc injected (n = 5 mice, 73 axons, green) and VTA injected (n = 5 mice, 98 axons, red) mice. Bottom, mean acceleration. **k,** Mean DF/F triggered on reward for all putative single axons in (**j**) from SNc (green) and VTA (red). Bottom, mean mouse licking triggered on reward delivery. **l,** Reward triggered DF/F for all putative VTA (left) and SNc (right) axons (same axons in **j–k**, sorted by reward response magnitude); each row represents mean DF/F for each axon. **m,** Mean DF/F triggered on acceleration onsets (top) and rewards (bottom) for all significant ($P < 0.01$) VTA reward responsive (n = 43 axons from 5 mice, red) and SNc locomotion responsive (n = 63 axons from 5 mice, green) axons. **n,** Reward response vs locomotion index for all VTA (n = 5 mice, top) and SNc (n = 5 mice, bottom) putative axons. Green, significant locomotion; red, significant reward; blue both significant; neither significant not shown. **o,** Mean DF/F during locomotion (top) and rest (bottom, non-reward periods during rest) periods for all locomotion (n = 19 axons, 4 mice green) and reward (n = 43 axons, 5 mice red) responsive VTA axons. **o**, *, $p < 10^{-5}$. Shaded regions in **j,k,m,** mean +/− s.e.m.

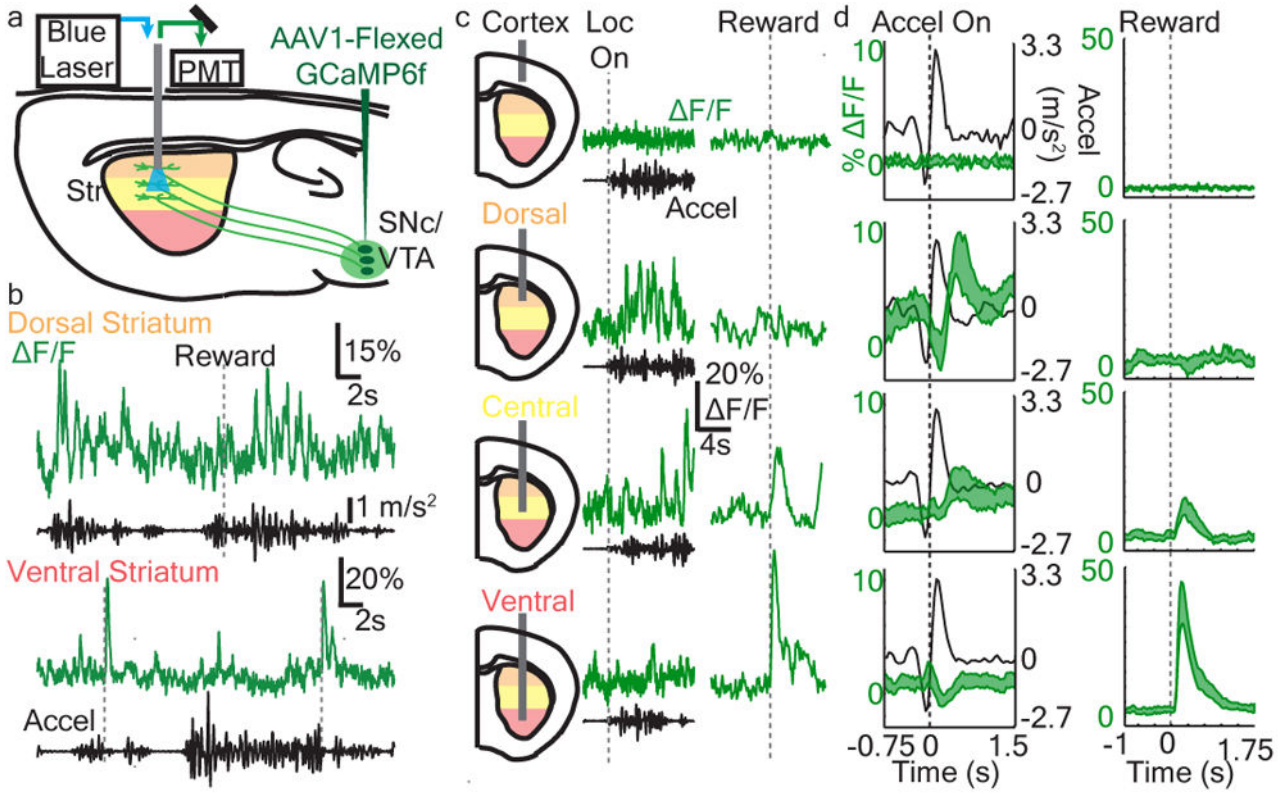

Fig 5. Functional topography of reward and locomotion dopamine signaling across striatum dorsal-ventral axis

a, Schematic of photometry methods. **b,** Representative photometry DF/F (green) and treadmill accelerations (black) during locomotion and reward delivery (dashed lines) periods from dorsal (top) and ventral (bottom) striatum from same mouse (same session, n = 5 mice total). **c,** Representative photometry DF/F from individual locomotion initiations (left column) and reward deliveries (right column) measured at indicated depths (not averaged). **d,** Mean DF/F across all photometry recording sessions (n = 5 mice) triggered on acceleration onsets (left) and reward deliveries (right) at depths indicated in **c** (black, mean acceleration).